3D INCOMPRESSIBLE NAVIER-STOKES EQUATIONS: COMPLEX BLOW-UP AND RELATED REAL FLOWS

3D INCOMPRESSIBLE NAVIER-STOKES EQUATIONS: COMPLEX BLOW-UP AND RELATED REAL FLOWS

C. Boldrighini

Istituto Nazionale d'Alta Matematica, GNFM, unità locale Roma III

3D INCOMPRESSIBLE NAVIER-STOKES EQUATIONS: COMPLEX BLOW-UP AND RELATED REAL FLOWS

C. Boldrighini

Istituto Nazionale d'Alta Matematica, GNFM, unità locale Roma III

Work in collaboration with

S. Frigio and P. Maponi,

Università di Camerino

3D INCOMPRESSIBLE NAVIER-STOKES EQUATIONS: COMPLEX BLOW-UP AND RELATED REAL FLOWS

C. Boldrighini

Istituto Nazionale d'Alta Matematica, GNFM, unità locale Roma III

Work in collaboration with

S. Frigio and P. Maponi,

Università di Camerino

A. Pellegrinotti,

Università di Roma III

Ya. G. Sinai,

Princeton University and Russian Academy of Sciences

XI International Conference of Mathematical Physics in Armenia

"Stochastic and Analytic Methods in Mathematical Physics"

Yerevan, Armenia, September 2-7 2019

Dedicated to the memory of Robert A.Minlos

1. INTRODUCTION

We consider the three-dimensional incompressible Navier-Stokes (NS) equations, in absence of boundary conditions and external forces:

1. INTRODUCTION

We consider the three-dimensional incompressible Navier-Stokes (NS) equations, in absence of boundary conditions and external forces:

$$\frac{\partial \mathbf{u}}{\partial t} + \sum_{j=1}^{3} u_j \frac{\partial}{\partial x_j}\mathbf{u} = \Delta \mathbf{u} - \nabla p, \qquad \mathbf{x} = (x_1, x_2, x_3) \in \mathbb{R}^3.$$

$$\nabla \cdot \mathbf{u} = 0, \qquad \mathbf{u}(\cdot, 0) = \mathbf{u}_0.$$

$\mathbf{u} : \mathbb{R}^3 \times [0, \infty) \to \mathbb{R}^3$ is the velocity field, p is the pressure and we assume for the viscosity $\nu = 1$ (always possible by rescaling).

1. INTRODUCTION

We consider the three-dimensional incompressible Navier-Stokes (NS) equations, in absence of boundary conditions and external forces:

$$\frac{\partial \mathbf{u}}{\partial t} + \sum_{j=1}^{3} u_j \frac{\partial}{\partial x_j}\mathbf{u} = \Delta \mathbf{u} - \nabla p, \qquad \mathbf{x} = (x_1, x_2, x_3) \in \mathbb{R}^3.$$

$$\nabla \cdot \mathbf{u} = 0, \qquad \mathbf{u}(\cdot, 0) = \mathbf{u}_0.$$

$\mathbf{u} : \mathbb{R}^3 \times [0, \infty) \to \mathbb{R}^3$ is the velocity field, p is the pressure and we assume for the viscosity $\nu = 1$ (always possible by rescaling).

In spite of considerable progress, it is still unknown whether there are smooth solutions that become singular in a finite time.

1. INTRODUCTION

We consider the three-dimensional incompressible Navier-Stokes (NS) equations, in absence of boundary conditions and external forces:

$$\frac{\partial \mathbf{u}}{\partial t} + \sum_{j=1}^{3} u_j \frac{\partial}{\partial x_j}\mathbf{u} = \Delta \mathbf{u} - \nabla p, \qquad \mathbf{x} = (x_1, x_2, x_3) \in \mathbb{R}^3.$$

$$\nabla \cdot \mathbf{u} = 0, \qquad \mathbf{u}(\cdot, 0) = \mathbf{u}_0.$$

$\mathbf{u} : \mathbb{R}^3 \times [0, \infty) \to \mathbb{R}^3$ is the velocity field, p is the pressure and we assume for the viscosity $\nu = 1$ (always possible by rescaling).

In spite of considerable progress, it is still unknown whether there are smooth solutions that become singular in a finite time. This is the celebrated Global Regularity Problem (GRP), in the list of the Clay millennium problems.

The problem begins in 1937 with Jean Leray,

The problem begins in 1937 with Jean Leray, who first proved a global weak existence theorem and a uniqueness and regularity theorem only for finite times.

The problem begins in 1937 with Jean Leray, who first proved a global weak existence theorem and a uniqueness and regularity theorem only for finite times. He believed that the loss of regularity and uniqueness is related to turbulence.

The problem begins in 1937 with Jean Leray, who first proved a global weak existence theorem and a uniqueness and regularity theorem only for finite times. He believed that the loss of regularity and uniqueness is related to turbulence.

The modern view of turbulence is not based on singularities,

The problem begins in 1937 with Jean Leray, who first proved a global weak existence theorem and a uniqueness and regularity theorem only for finite times. He believed that the loss of regularity and uniqueness is related to turbulence.

The modern view of turbulence is not based on singularities, rather to transitions to chaotic flows.

The problem begins in 1937 with Jean Leray, who first proved a global weak existence theorem and a uniqueness and regularity theorem only for finite times. He believed that the loss of regularity and uniqueness is related to turbulence.

The modern view of turbulence is not based on singularities, rather to transitions to chaotic flows.

Already Leray proved that if a solution becomes singular at some time τ, then the total enstrophy

$$S(t) = \int_{\mathbb{R}^3} |\omega(\mathbf{x}, t)|^2 d\mathbf{x},$$

where $\omega(\mathbf{x}, t) = \nabla \times \mathbf{u}(\mathbf{x}, t)$ is the vorticity, diverges as $t \uparrow \tau$;

The problem begins in 1937 with Jean Leray, who first proved a global weak existence theorem and a uniqueness and regularity theorem only for finite times. He believed that the loss of regularity and uniqueness is related to turbulence.

The modern view of turbulence is not based on singularities, rather to transitions to chaotic flows.

Already Leray proved that if a solution becomes singular at some time τ, then the total enstrophy

$$S(t) = \int_{\mathbb{R}^3} |\omega(\mathbf{x}, t)|^2 d\mathbf{x},$$

where $\omega(\mathbf{x}, t) = \nabla \times \mathbf{u}(\mathbf{x}, t)$ is the vorticity, diverges as $t \uparrow \tau$; i.e., the support in Fourier $\mathbf{k}$-space moves to the high $|\mathbf{k}|$ region.

More recently it was established that the absolute value of the velocity at some space point also diverges as $t \uparrow \tau$ (*G. Seregin, 2012*).

More recently it was established that the absolute value of the velocity at some space point also diverges as $t \uparrow \tau$ (*G. Seregin, 2012*).

Therefore the singularities, if they exist, could describe physical phenomena, such as sudden concentrations of energy in a finite space region, as it happens in tornadoes or hurricanes, for which no effective model is now available.

More recently it was established that the absolute value of the velocity at some space point also diverges as $t \uparrow \tau$ (*G. Seregin, 2012*).

Therefore the singularities, if they exist, could describe physical phenomena, such as sudden concentrations of energy in a finite space region, as it happens in tornadoes or hurricanes, for which no effective model is now available.

The energy equality

$$E(t) + \int_0^t S(\tau) d\tau = E(0),$$

More recently it was established that the absolute value of the velocity at some space point also diverges as $t \uparrow \tau$ (*G. Seregin, 2012*).

Therefore the singularities, if they exist, could describe physical phenomena, such as sudden concentrations of energy in a finite space region, as it happens in tornadoes or hurricanes, for which no effective model is now available.

The energy equality

$$E(t) + \int_0^t S(\tau) d\tau = E(0),$$

shows that the total energy $E(t)$ decreases, and any divergence of $S(t)$ has to be integrable.

Opinions with regard to the GRP differ.

Opinions with regard to the GRP differ.

Proofs of a finite-time blow-up were obtained for some variants of the dyadic model *(A. Cheskidov 2008)*, a discrete simplification of the NS equations which preserves energy conservation,

Opinions with regard to the GRP differ.

Proofs of a finite-time blow-up were obtained for some variants of the dyadic model *(A. Cheskidov 2008)*, a discrete simplification of the NS equations which preserves energy conservation, first considered by Katz and Pavlovic (*N. K. Katz & N. Pavlovic 2002*) for the Euler equations.

Opinions with regard to the GRP differ.

Proofs of a finite-time blow-up were obtained for some variants of the dyadic model *(A. Cheskidov 2008)*, a discrete simplification of the NS equations which preserves energy conservation, first considered by Katz and Pavlovic (*N. K. Katz & N. Pavlovic 2002*) for the Euler equations.
(Origin: shell model for the energy cascade of turbulence.)

T. Tao proved in a paper of 2016 a finite-time blow-up for a NS system with a modified bilinear term satisfying the energy identity (*T. Tao 2016*).

Opinions with regard to the GRP differ.

Proofs of a finite-time blow-up were obtained for some variants of the dyadic model *(A. Cheskidov 2008)*, a discrete simplification of the NS equations which preserves energy conservation, first considered by Katz and Pavlovic (*N. K. Katz & N. Pavlovic 2002*) for the Euler equations.
(Origin: shell model for the energy cascade of turbulence.)

T. Tao proved in a paper of 2016 a finite-time blow-up for a NS system with a modified bilinear term satisfying the energy identity (*T. Tao 2016*).
The modification follows the lines of the dyadic model.

The evidence from computer simulations is inconclusive:

The evidence from computer simulations is inconclusive: a theoretical guideline is needed in order to control the difficulties arising in computing solutions of the three-dimensional NS equations for high values of the velocity and the vorticity.

The evidence from computer simulations is inconclusive: a theoretical guideline is needed in order to control the difficulties arising in computing solutions of the three-dimensional NS equations for high values of the velocity and the vorticity.

In 2008 Li and Sinai *(Li & Sinai, 2008)* proved that there are solutions of the NS equation in 3D with no external forces which do indeed blow up after a finite time for some class of smooth initial data.

The evidence from computer simulations is inconclusive: a theoretical guideline is needed in order to control the difficulties arising in computing solutions of the three-dimensional NS equations for high values of the velocity and the vorticity.

In 2008 Li and Sinai *(Li & Sinai, 2008)* proved that there are solutions of the NS equation in 3D with no external forces which do indeed blow up after a finite time for some class of smooth initial data. Their work relies on the application of ideas and methods inspired by the theory of dynamical systems.

The evidence from computer simulations is inconclusive: a theoretical guideline is needed in order to control the difficulties arising in computing solutions of the three-dimensional NS equations for high values of the velocity and the vorticity.

In 2008 Li and Sinai *(Li & Sinai, 2008)* proved that there are solutions of the NS equation in 3D with no external forces which do indeed blow up after a finite time for some class of smooth initial data. Their work relies on the application of ideas and methods inspired by the theory of dynamical systems.

The solutions of Li and Sinai are unphysical: the energy diverges (The energy identity holds but is not coercive.)

The evidence from computer simulations is inconclusive: a theoretical guideline is needed in order to control the difficulties arising in computing solutions of the three-dimensional NS equations for high values of the velocity and the vorticity.

In 2008 Li and Sinai *(Li & Sinai, 2008)* proved that there are solutions of the NS equation in 3D with no external forces which do indeed blow up after a finite time for some class of smooth initial data. Their work relies on the application of ideas and methods inspired by the theory of dynamical systems.

The solutions of Li and Sinai are unphysical: the energy diverges (The energy identity holds but is not coercive.)

They suggest however the study of a new class of real flows which is interesting in itself and may be relevant for the GRP.

2. LI-SINAI SOLUTIONS

Similar complex solutions with blow-up have been established for the Burgers equations and other models (*Li & Sinai 2010*).

2. LI-SINAI SOLUTIONS

Similar complex solutions with blow-up have been established for the Burgers equations and other models (*Li & Sinai 2010*).

The starting point is a reformulation of the 3D NS equations into a convolution integral equation.

2. LI-SINAI SOLUTIONS

Similar complex solutions with blow-up have been established for the Burgers equations and other models (*Li & Sinai 2010*).

The starting point is a reformulation of the 3D NS equations into a convolution integral equation. Let

$$\mathbf{v}(\mathbf{k},t) = \frac{i}{(2\pi)^3}\int_{\mathbb{R}^3}\mathbf{u}(\mathbf{x},t)e^{i(\mathbf{k},x)}d\mathbf{x}.$$

The NS equations go, by a Duhamel formula, into

$$\mathbf{v}(\mathbf{k},t) = e^{-t\mathbf{k}^2}\mathbf{v}_0(\mathbf{k}) +$$

$$+\int_0^t e^{-(t-s)\mathbf{k}^2}ds\int_{\mathbb{R}^3}\langle\mathbf{v}(\mathbf{k}-\mathbf{k}',s),\mathbf{k}\rangle\ P_{\mathbf{k}}\ \mathbf{v}(\mathbf{k}',s)\ d\mathbf{k}',$$

2. LI-SINAI SOLUTIONS

Similar complex solutions with blow-up have been established for the Burgers equations and other models (*Li & Sinai 2010*).

The starting point is a reformulation of the 3D NS equations into a convolution integral equation. Let

$$\mathbf{v}(\mathbf{k},t) = \frac{i}{(2\pi)^3}\int_{\mathbb{R}^3}\mathbf{u}(\mathbf{x},t)e^{i(\mathbf{k},x)}d\mathbf{x}.$$

The NS equations go, by a Duhamel formula, into

$$\mathbf{v}(\mathbf{k},t) = e^{-t\mathbf{k}^2}\mathbf{v}_0(\mathbf{k}) +$$

$$+\int_0^t e^{-(t-s)\mathbf{k}^2}ds\int_{\mathbb{R}^3}\langle\mathbf{v}(\mathbf{k}-\mathbf{k}',s),\mathbf{k}\rangle\ P_{\mathbf{k}}\ \mathbf{v}(\mathbf{k}',s)\ d\mathbf{k}',$$

where $\mathbf{v}_0(\mathbf{k}) = \mathbf{v}(\mathbf{k},0)$ is the initial data and $P_{\mathbf{k}}$ the orthogonal projector expressing incompressibility: $P_{\mathbf{k}}\mathbf{v} = \mathbf{v} - \frac{\langle\mathbf{v},\mathbf{k}\rangle}{\mathbf{k}^2}\mathbf{k}$.

Only real solutions $\mathbf{v}(\mathbf{k}, t)$ are considered. The velocity in physical space $\mathbf{u}(\mathbf{x}, t)$ is complex in general.

2. Li-Sinai solutions 2

Only real solutions $\mathbf{v}(\mathbf{k}, t)$ are considered. The velocity in physical space $\mathbf{u}(\mathbf{x}, t)$ is complex in general.

If however $\mathbf{v}(\mathbf{k}, t)$ is odd in $\mathbf{k}$ then $\mathbf{u}(\mathbf{x}, t)$ is real and describes a NS flow which is odd in $\mathbf{x}$.

Only real solutions $\mathbf{v}(\mathbf{k}, t)$ are considered. The velocity in physical space $\mathbf{u}(\mathbf{x}, t)$ is complex in general.

If however $\mathbf{v}(\mathbf{k}, t)$ is odd in $\mathbf{k}$ then $\mathbf{u}(\mathbf{x}, t)$ is real and describes a NS flow which is odd in $\mathbf{x}$.

It is convenient to represent the solution as a power series by introducing a real parameter A.

Only real solutions $\mathbf{v}(\mathbf{k}, t)$ are considered. The velocity in physical space $\mathbf{u}(\mathbf{x}, t)$ is complex in general.

If however $\mathbf{v}(\mathbf{k}, t)$ is odd in $\mathbf{k}$ then $\mathbf{u}(\mathbf{x}, t)$ is real and describes a NS flow which is odd in $\mathbf{x}$.

It is convenient to represent the solution as a power series by introducing a real parameter A. Taking the initial data $\mathbf{v}_A(\mathbf{k}, 0) = A\mathbf{v}_0$, we obtain a series of the form

$$\mathbf{v}_A(\mathbf{k}, t) = Ae^{-t\mathbf{k}^2}\mathbf{v}_0(\mathbf{k}) + \int_0^t e^{-(t-s)\mathbf{k}^2} \sum_{p=2}^{\infty} A^p \mathbf{g}^{(p)}(\mathbf{k}, s) ds.$$

Only real solutions $\mathbf{v}(\mathbf{k}, t)$ are considered. The velocity in physical space $\mathbf{u}(\mathbf{x}, t)$ is complex in general.

If however $\mathbf{v}(\mathbf{k}, t)$ is odd in $\mathbf{k}$ then $\mathbf{u}(\mathbf{x}, t)$ is real and describes a NS flow which is odd in $\mathbf{x}$.

It is convenient to represent the solution as a power series by introducing a real parameter A. Taking the initial data $\mathbf{v}_A(\mathbf{k}, 0) = A\mathbf{v}_0$, we obtain a series of the form

$$\mathbf{v}_A(\mathbf{k}, t) = Ae^{-t\mathbf{k}^2}\mathbf{v}_0(\mathbf{k}) + \int_0^t e^{-(t-s)\mathbf{k}^2} \sum_{p=2}^{\infty} A^p \mathbf{g}^{(p)}(\mathbf{k}, s) ds.$$

$$\mathbf{g}^{(1)}(\mathbf{k}, s) = e^{-s\mathbf{k}^2}\mathbf{v}_0(\mathbf{k})$$

$$\mathbf{g}^{(2)}(\mathbf{k}, s) = \int_{\mathbb{R}^3} \left\langle \mathbf{v}_0(\mathbf{k} - \mathbf{k}'), \mathbf{k} \right\rangle P_{\mathbf{k}}\mathbf{v}_0(\mathbf{k}')\, e^{-s(\mathbf{k}-\mathbf{k}')^2 - s(\mathbf{k}')^2} d\mathbf{k}',$$

For $p > 2$ we have the recursive relation

$$\mathbf{g}^{(p)}(\mathbf{k}, s) =$$

$$= \int_0^s ds_2 \int_{\mathbb{R}^3} \left\langle \mathbf{v}_0(k - k'), \mathbf{k} \right\rangle \; P_{\mathbf{k}} \mathbf{g}^{(p-1)}(\mathbf{k}', s_2) e^{-s(\mathbf{k}-\mathbf{k}')^2 - (s-s_2)(\mathbf{k}')^2} d\mathbf{k}' +$$

$$+ \sum_{\substack{p_1+p_2=p \\ p_1,p_2>1}} \int_0^s ds_1 \int_0^s ds_2 \int_{\mathbb{R}^3} \left\langle \mathbf{g}^{(p_1)}(\mathbf{k} - \mathbf{k}', s_1), \mathbf{k} \right\rangle \cdot$$

$$\cdot P_{\mathbf{k}} \mathbf{g}^{(p_2)}(\mathbf{k}', s_2) e^{-(s-s_1)(\mathbf{k}-\mathbf{k}')^2 - (s-s_2)(\mathbf{k}')^2} d\mathbf{k}' +$$

$$+ \int_0^s ds_1 \int_{\mathbb{R}^3} \left\langle \mathbf{g}^{(p-1)}(\mathbf{k} - \mathbf{k}', s_1), \mathbf{k} \right\rangle \; P_{\mathbf{k}} \mathbf{v}_0(\mathbf{k}') e^{-(s-s_1)(\mathbf{k}-\mathbf{k}')^2 - s(\mathbf{k}')^2} d\mathbf{k}'.$$

For $p > 2$ we have the recursive relation

$$\mathbf{g}^{(p)}(\mathbf{k}, s) =$$

$$= \int_0^s ds_2 \int_{\mathbb{R}^3} \left\langle \mathbf{v}_0(k - k'), \mathbf{k} \right\rangle \; P_{\mathbf{k}} \mathbf{g}^{(p-1)}(\mathbf{k}', s_2) e^{-s(\mathbf{k}-\mathbf{k}')^2 - (s-s_2)(\mathbf{k}')^2} d\mathbf{k}' +$$

$$+ \sum_{\substack{p_1+p_2=p \\ p_1,p_2>1}} \int_0^s ds_1 \int_0^s ds_2 \int_{\mathbb{R}^3} \left\langle \mathbf{g}^{(p_1)}(\mathbf{k} - \mathbf{k}', s_1), \mathbf{k} \right\rangle \cdot$$

$$\cdot P_{\mathbf{k}} \mathbf{g}^{(p_2)}(\mathbf{k}', s_2) e^{-(s-s_1)(\mathbf{k}-\mathbf{k}')^2 - (s-s_2)(\mathbf{k}')^2} d\mathbf{k}' +$$

$$+ \int_0^s ds_1 \int_{\mathbb{R}^3} \left\langle \mathbf{g}^{(p-1)}(\mathbf{k} - \mathbf{k}', s_1), \mathbf{k} \right\rangle \; P_{\mathbf{k}} \mathbf{v}_0(\mathbf{k}') e^{-(s-s_1)(\mathbf{k}-\mathbf{k}')^2 - s(\mathbf{k}')^2} d\mathbf{k}'.$$

It can be shown that if $\mathbf{v}_0$ is bounded and summable, the series converge for t small (depending on A).

The Li-Sinai theory considers initial data $\mathbf{v}_0$ with essential support in a sphere D of radius R around a point $\mathbf{k}^{(0)} \neq 0$, with $R << |\mathbf{k}^{(0)}|$. For definiteness assume $\mathbf{k}^{(0)} = (0, 0, a)$, $a > 0$.

The Li-Sinai theory considers initial data $\mathbf{v}_0$ with essential support in a sphere D of radius R around a point $\mathbf{k}^{(0)} \neq 0$, with $R << |\mathbf{k}^{(0)}|$. For definiteness assume $\mathbf{k}^{(0)} = (0, 0, a)$, $a > 0$.

By way of convolution, the support of $\mathbf{g}^{(p)}$ will be $\underbrace{D + \ldots + D}_{p \text{ times}}$,

which is centered around $p\mathbf{k}^{(0)}$, and, for large p, by analogy with probability theory, has a transversal dimension of the order $\sqrt{p}$.

The Li-Sinai theory considers initial data $\mathbf{v}_0$ with essential support in a sphere D of radius R around a point $\mathbf{k}^{(0)} \neq 0$, with $R << |\mathbf{k}^{(0)}|$. For definiteness assume $\mathbf{k}^{(0)} = (0, 0, a)$, $a > 0$.

By way of convolution, the support of $\mathbf{g}^{(p)}$ will be $\underbrace{D + \ldots + D}_{p \text{ times}}$,

which is centered around $p\mathbf{k}^{(0)}$, and, for large p, by analogy with probability theory, has a transversal dimension of the order $\sqrt{p}$.

The particular choice of $\mathbf{v}_0$ gives a control on the extension of the support to the high $|\mathbf{k}|$-values, which determine the fine structure of the real flows.

The Li-Sinai theory considers initial data $\mathbf{v}_0$ with essential support in a sphere D of radius R around a point $\mathbf{k}^{(0)} \neq 0$, with $R << |\mathbf{k}^{(0)}|$. For definiteness assume $\mathbf{k}^{(0)} = (0, 0, a)$, $a > 0$.

By way of convolution, the support of $\mathbf{g}^{(p)}$ will be $\underbrace{D + \ldots + D}_{p \text{ times}}$,

which is centered around $p\mathbf{k}^{(0)}$, and, for large p, by analogy with probability theory, has a transversal dimension of the order $\sqrt{p}$.

The particular choice of $\mathbf{v}_0$ gives a control on the extension of the support to the high $|\mathbf{k}|$-values, which determine the fine structure of the real flows.

We then introduce normalized variables and new functions:

$$\mathbf{k} = p\mathbf{k}^{(0)} + \sqrt{p}\,\mathbf{Y}^{(p)}, \qquad \mathbf{h}^{(p)}(\mathbf{Y}^{(p)}, s) = \mathbf{g}^{(p)}(p\mathbf{k}^{(0)} + \sqrt{p}\,\mathbf{Y}^{(p)}, s)$$

The Li-Sinai theory considers initial data $\mathbf{v}_0$ with essential support in a sphere D of radius R around a point $\mathbf{k}^{(0)} \neq 0$, with $R << |\mathbf{k}^{(0)}|$. For definiteness assume $\mathbf{k}^{(0)} = (0, 0, a)$, $a > 0$.

By way of convolution, the support of $\mathbf{g}^{(p)}$ will be $\underbrace{D + \ldots + D}_{p \text{ times}}$,

which is centered around $p\mathbf{k}^{(0)}$, and, for large p, by analogy with probability theory, has a transversal dimension of the order $\sqrt{p}$.

The particular choice of $\mathbf{v}_0$ gives a control on the extension of the support to the high $|\mathbf{k}|$-values, which determine the fine structure of the real flows.

We then introduce normalized variables and new functions:

$$\mathbf{k} = p\mathbf{k}^{(0)} + \sqrt{p}\,\mathbf{Y}^{(p)}, \qquad \mathbf{h}^{(p)}(\mathbf{Y}^{(p)}, s) = \mathbf{g}^{(p)}(p\mathbf{k}^{(0)} + \sqrt{p}\,\mathbf{Y}^{(p)}, s)$$

where $\mathbf{Y}^{(p)} = \mathcal{O}(1)$.

2. Li-Sinai solutions 5

If p is large one can see that the contribution to $\mathbf{g}^{(p)}$ of the sum of the terms with $\max\{p_1, p_2\} \leq p^{\frac{1}{2}}$ can be neglected.

2. Li-Sinai solutions 5

If p is large one can see that the contribution to $\mathbf{g}^{(p)}$ of the sum of the terms with $\max\{p_1, p_2\} \leq p^{\frac{1}{2}}$ can be neglected.

Neglecting the boundary terms, setting

$$s_j = s\left(1 - \frac{\theta_j}{p_j^2}\right), \qquad j = 1, 2,$$

2. Li-Sinai solutions 5

If p is large one can see that the contribution to $\mathbf{g}^{(p)}$ of the sum of the terms with $\max\{p_1, p_2\} \leq p^{\frac{1}{2}}$ can be neglected.

Neglecting the boundary terms, setting

$$s_j = s\left(1 - \frac{\theta_j}{p_j^2}\right), \qquad j = 1, 2,$$

integrating over $\theta_j, j = 1, 2$ and observing that the main contribution of the exponential factors to the integrals comes for $s_1, s_2 \approx s$ we get a simplified recursive relation ($\mathbf{Y}^{(p)} = \mathbf{Y}$)

If p is large one can see that the contribution to $\mathbf{g}^{(p)}$ of the sum of the terms with $\max\{p_1, p_2\} \leq p^{\frac{1}{2}}$ can be neglected.

Neglecting the boundary terms, setting

$$s_j = s\left(1 - \frac{\theta_j}{p_j^2}\right), \qquad j = 1, 2,$$

integrating over $\theta_j, j = 1, 2$ and observing that the main contribution of the exponential factors to the integrals comes for $s_1, s_2 \approx s$ we get a simplified recursive relation ($\mathbf{Y}^{(p)} = \mathbf{Y}$)

$$\mathbf{h}^{(p)}(\mathbf{Y}, s) = p^{\frac{5}{2}} \sum_{\substack{p_1+p_2=p \\ p_1,p_2>\sqrt{p}}} \frac{1}{p_1^2 p_2^2} \int_{\mathbb{R}^3} P_{\mathbf{e}_3+\frac{\mathbf{Y}}{\sqrt{p}}}\, \mathbf{h}^{(p_2)}\left(\frac{\mathbf{Y}'}{\sqrt{1-\gamma}}, s\right) \cdot$$

$$\cdot \left\langle \mathbf{h}^{(p_1)}\left(\frac{\mathbf{Y}-\mathbf{Y}'}{\sqrt{\gamma}}, s\right), \mathbf{e}_3 + \frac{\mathbf{Y}}{\sqrt{p}} \right\rangle d\mathbf{Y}',$$

where $\mathbf{e}_3$ is the unit vector along the k_3 axis.

As $\mathbf{k} = p\mathbf{k}^{(0)} + \mathbf{Y}$, the incompressibility condition

$$\langle \mathbf{h}^{(p)}(\mathbf{Y}, s), \mathbf{k} \rangle = \langle \mathbf{h}^{(p)}(\mathbf{Y}, s), pa\, \mathbf{e}_3 + \sqrt{p}\mathbf{Y} \rangle = 0$$

implies for the third component of $\mathbf{h}^{(p)}$

$$h_3^{(p)} = -\frac{1}{ap} F^{(p)}(\mathbf{Y}, s), \qquad F^{(p)}(\mathbf{Y}, s) = \langle \mathbf{h}^{(p)}(\mathbf{Y}, s), \mathbf{Y} \rangle = \mathcal{O}(1),$$

i.e., $h_3^{(p)}(\mathbf{Y}, s) = \mathcal{O}(p^{-\frac{1}{2}})$.

As $\mathbf{k} = p\mathbf{k}^{(0)} + \mathbf{Y}$, the incompressibility condition

$$\langle \mathbf{h}^{(p)}(\mathbf{Y}, s), \mathbf{k} \rangle = \langle \mathbf{h}^{(p)}(\mathbf{Y}, s), pa\, \mathbf{e}_3 + \sqrt{p}\mathbf{Y} \rangle = 0$$

implies for the third component of $\mathbf{h}^{(p)}$

$$h_3^{(p)} = -\frac{1}{ap} F^{(p)}(\mathbf{Y}, s), \qquad F^{(p)}(\mathbf{Y}, s) = \langle \mathbf{h}^{(p)}(\mathbf{Y}, s), \mathbf{Y} \rangle = \mathcal{O}(1),$$

i.e., $h_3^{(p)}(\mathbf{Y}, s) = \mathcal{O}(p^{-\frac{1}{2}})$. Hence if p is large, the vector $\mathbf{h}^{(p)}(\mathbf{Y}, s)$ is essentially transversal to the $\mathbf{e}_3$-axis,

As $\mathbf{k} = p\mathbf{k}^{(0)} + \mathbf{Y}$, the incompressibility condition

$$\langle \mathbf{h}^{(p)}(\mathbf{Y}, s), \mathbf{k} \rangle = \langle \mathbf{h}^{(p)}(\mathbf{Y}, s), pa\, \mathbf{e}_3 + \sqrt{p}\mathbf{Y} \rangle = 0$$

implies for the third component of $\mathbf{h}^{(p)}$

$$h_3^{(p)} = -\frac{1}{ap} F^{(p)}(\mathbf{Y}, s), \qquad F^{(p)}(\mathbf{Y}, s) = \langle \mathbf{h}^{(p)}(\mathbf{Y}, s), \mathbf{Y} \rangle = \mathcal{O}(1),$$

i.e., $h_3^{(p)}(\mathbf{Y}, s) = \mathcal{O}(p^{-\frac{1}{2}})$. Hence if p is large, the vector $\mathbf{h}^{(p)}(\mathbf{Y}, s)$ is essentially transversal to the $\mathbf{e}_3$-axis, and in the recurrence relation the projection $P_{\mathbf{e}_3 + \frac{\mathbf{Y}}{\sqrt{p}}}\, \mathbf{h}^{(p_2)}$ may be replaced by $\mathbf{h}^{(p_2)}$.

As $\mathbf{k} = p\mathbf{k}^{(0)} + \mathbf{Y}$, the incompressibility condition

$$\langle \mathbf{h}^{(p)}(\mathbf{Y}, s), \mathbf{k} \rangle = \langle \mathbf{h}^{(p)}(\mathbf{Y}, s), pa\, \mathbf{e}_3 + \sqrt{p}\mathbf{Y} \rangle = 0$$

implies for the third component of $\mathbf{h}^{(p)}$

$$h_3^{(p)} = -\frac{1}{ap} F^{(p)}(\mathbf{Y}, s), \qquad F^{(p)}(\mathbf{Y}, s) = \langle \mathbf{h}^{(p)}(\mathbf{Y}, s), \mathbf{Y} \rangle = \mathcal{O}(1),$$

i.e., $h_3^{(p)}(\mathbf{Y}, s) = \mathcal{O}(p^{-\frac{1}{2}})$. Hence if p is large, the vector $\mathbf{h}^{(p)}(\mathbf{Y}, s)$ is essentially transversal to the $\mathbf{e}_3$-axis, and in the recurrence relation the projection $P_{\mathbf{e}_3 + \frac{\mathbf{Y}}{\sqrt{p}}}\, \mathbf{h}^{(p_2)}$ may be replaced by $\mathbf{h}^{(p_2)}$.

We get a remarkable simplification: *the incompressibility projector is reduced to the identity.*

The fundamental *Ansatz*, suggested by the CLT of probability, is that for p large enough and s in some interval, the solution of the recursive relation has the form

$$\mathbf{h}^{(p)}(\mathbf{Y}, s) = p(\Lambda(s))^p g^{(3)}(\mathbf{Y}) \left(\mathbf{H}(\mathbf{Y}) + \delta^{(p)}(\mathbf{Y}, s) \right)$$

The fundamental *Ansatz*, suggested by the CLT of probability, is that for p large enough and s in some interval, the solution of the recursive relation has the form

$$\mathbf{h}^{(p)}(\mathbf{Y}, s) = p(\Lambda(s))^p g^{(3)}(\mathbf{Y}) \left(\mathbf{H}(\mathbf{Y}) + \delta^{(p)}(\mathbf{Y}, s) \right)$$

where $g^{(3)}(\mathbf{Y})$ is the standard Gaussian in $\mathbb{R}^3$, the function Λ and the function $\mathbf{H}(\mathbf{Y}) = (H_1(\mathbf{Y}),\ H_2(\mathbf{Y}), 0)$,

The fundamental *Ansatz*, suggested by the CLT of probability, is that for p large enough and s in some interval, the solution of the recursive relation has the form

$$\mathbf{h}^{(p)}(\mathbf{Y}, s) = p(\Lambda(s))^p g^{(3)}(\mathbf{Y}) \left(\mathbf{H}(\mathbf{Y}) + \delta^{(p)}(\mathbf{Y}, s) \right)$$

where $g^{(3)}(\mathbf{Y})$ is the standard Gaussian in $\mathbb{R}^3$, the function Λ and the function $\mathbf{H}(\mathbf{Y}) = (H_1(\mathbf{Y}),\ H_2(\mathbf{Y}), 0)$, *which should be a fixed point for the map* $\mathbf{h}^{(p)} \to \mathbf{h}^{(p+1)}$, depending only on $\mathbf{Y}^\perp := (Y_1, Y_2)$, are to be determined, and the remainder $\delta^{(p)}(\mathbf{Y}, s)$ vanishes for large p:

The fundamental *Ansatz*, suggested by the CLT of probability, is that for p large enough and s in some interval, the solution of the recursive relation has the form

$$\mathbf{h}^{(p)}(\mathbf{Y}, s) = p(\Lambda(s))^p g^{(3)}(\mathbf{Y}) \left(\mathbf{H}(\mathbf{Y}) + \delta^{(p)}(\mathbf{Y}, s) \right)$$

where $g^{(3)}(\mathbf{Y})$ is the standard Gaussian in $\mathbb{R}^3$, the function Λ and the function $\mathbf{H}(\mathbf{Y}) = (H_1(\mathbf{Y}),\ H_2(\mathbf{Y}), 0)$, *which should be a fixed point for the map* $\mathbf{h}^{(p)} \to \mathbf{h}^{(p+1)}$, depending only on $\mathbf{Y}^{\perp} := (Y_1, Y_2)$, are to be determined, and the remainder $\delta^{(p)}(\mathbf{Y}, s)$ vanishes for large p:

$$\delta^{(p)}(\mathbf{Y}, s) = \left(\delta_1^{(p)}(\mathbf{Y}, s), \delta_2^{(p)}(\mathbf{Y}, s), \delta_3^{(p)}(\mathbf{Y}, s) \right) \to 0, \qquad p \to \infty.$$

The fundamental *Ansatz*, suggested by the CLT of probability, is that for p large enough and s in some interval, the solution of the recursive relation has the form

$$\mathbf{h}^{(p)}(\mathbf{Y}, s) = p(\Lambda(s))^p g^{(3)}(\mathbf{Y}) \left(\mathbf{H}(\mathbf{Y}) + \delta^{(p)}(\mathbf{Y}, s) \right)$$

where $g^{(3)}(\mathbf{Y})$ is the standard Gaussian in $\mathbb{R}^3$, the function Λ and the function $\mathbf{H}(\mathbf{Y}) = (H_1(\mathbf{Y}),\ H_2(\mathbf{Y}), 0)$, *which should be a fixed point for the map* $\mathbf{h}^{(p)} \to \mathbf{h}^{(p+1)}$, depending only on $\mathbf{Y}^\perp := (Y_1, Y_2)$, are to be determined, and the remainder $\delta^{(p)}(\mathbf{Y}, s)$ vanishes for large p:

$$\delta^{(p)}(\mathbf{Y}, s) = \left(\delta_1^{(p)}(\mathbf{Y}, s), \delta_2^{(p)}(\mathbf{Y}, s), \delta_3^{(p)}(\mathbf{Y}, s) \right) \to 0, \qquad p \to \infty.$$

(The correlation matrix of the Gaussian depends on $\mathbf{v}_0$: we assume for simplicity that it is standard.)

Integrating over Y_3, and replacing the sum over p_1, p_2 by an integral over $\gamma = p_1/p$, we get, as $p \to \infty$, an integral equation for the fixed-point $\mathbf{H} : \mathbb{R}^2 \to \mathbb{R}^2$

Integrating over Y_3, and replacing the sum over p_1, p_2 by an integral over $\gamma = p_1/p$, we get, as $p \to \infty$, an integral equation for the fixed-point $\mathbf{H} : \mathbb{R}^2 \to \mathbb{R}^2$

$$g^{(2)}(\mathbf{Y})\mathbf{H}(\mathbf{Y}) =$$

$$= \int_0^1 d\gamma \int_{\mathbb{R}^2} g_\gamma^{(2)}(\mathbf{Y} - \mathbf{Y}') g_{1-\gamma}^{(2)}(\mathbf{Y}')\, \mathcal{E}_{\mathbf{H}}(\gamma, \mathbf{Y}, \mathbf{Y}')\, \mathbf{H}\left(\frac{\mathbf{Y}'}{\sqrt{1-\gamma}}\right) d\mathbf{Y}'$$

where $g_\sigma^{(2)}(\mathbf{x}) = \frac{e^{-\frac{\mathbf{x}^2}{2\sigma}}}{2\pi\sigma}$, $\mathbf{x} \in \mathbb{R}^2$, $g^{(2)} = g_1^{(2)}$ and

$$\mathcal{E}_{\mathbf{H}}(\gamma, \mathbf{Y}, \mathbf{Y}') = -(1-\gamma)^{\frac{3}{2}} \left\langle \frac{\mathbf{Y} - \mathbf{Y}'}{\sqrt{\gamma}}, \mathbf{H}\left(\frac{\mathbf{Y} - \mathbf{Y}'}{\sqrt{\gamma}}\right) \right\rangle_2 +$$

$$+ \gamma^{\frac{1}{2}}(1-\gamma) \left\langle \frac{\mathbf{Y}'}{\sqrt{1-\gamma}}, \mathbf{H}\left(\frac{\mathbf{Y}'}{\sqrt{1-\gamma}}\right) \right\rangle_2,$$

By expanding $\mathbf{H}(\mathbf{Y})$, $\mathbf{Y} = (Y_1, Y_2)$, in the Hermite polynomials Li and Sinai proved that there are infinitely many solutions to the fixed-point equation.

By expanding $\mathbf{H}(\mathbf{Y})$, $\mathbf{Y} = (Y_1, Y_2)$, in the Hermite polynomials Li and Sinai proved that there are infinitely many solutions to the fixed-point equation.

Following their work we consider the particular solution

$$\mathbf{H}^{(0)}(\mathbf{Y}) = c\,\mathbf{Y}, = c\,(Y_1, Y_2)$$

where c is a constant.

By expanding $\mathbf{H}(\mathbf{Y})$, $\mathbf{Y} = (Y_1, Y_2)$, in the Hermite polynomials Li and Sinai proved that there are infinitely many solutions to the fixed-point equation.

Following their work we consider the particular solution

$$\mathbf{H}^{(0)}(\mathbf{Y}) = c\,\mathbf{Y}, = c\,(Y_1, Y_2)$$

where c is a constant.

The main result of Li and Sinai (2008) states that *one can find a 10-parameter families of initial data and a time interval* (S_-, S_+), *such that the fundamental Ansatz holds with* $\mathbf{H} = \mathbf{H}^{(0)}$ *for an open set of the parameters and all* $s \in (S_-, S_+)$.

By expanding $\mathbf{H}(\mathbf{Y})$, $\mathbf{Y} = (Y_1, Y_2)$, in the Hermite polynomials Li and Sinai proved that there are infinitely many solutions to the fixed-point equation.

Following their work we consider the particular solution

$$\mathbf{H}^{(0)}(\mathbf{Y}) = c\,\mathbf{Y}, = c\,(Y_1, Y_2)$$

where c is a constant.

The main result of Li and Sinai (2008) states that *one can find a 10-parameter families of initial data and a time interval* (S_-, S_+), *such that the fundamental Ansatz holds with* $\mathbf{H} = \mathbf{H}^{(0)}$ *for an open set of the parameters and all* $s \in (S_-, S_+)$.

The parameters are the components on the unstable (6-d) and neutral (4-d) linear spaces.

By expanding $\mathbf{H}(\mathbf{Y})$, $\mathbf{Y} = (Y_1, Y_2)$, in the Hermite polynomials Li and Sinai proved that there are infinitely many solutions to the fixed-point equation.

Following their work we consider the particular solution

$$\mathbf{H}^{(0)}(\mathbf{Y}) = c\,\mathbf{Y}, = c\,(Y_1, Y_2)$$

where c is a constant.

The main result of Li and Sinai (2008) states that *one can find a 10-parameter families of initial data and a time interval* (S_-, S_+), *such that the fundamental Ansatz holds with* $\mathbf{H} = \mathbf{H}^{(0)}$ *for an open set of the parameters and all* $s \in (S_-, S_+)$.

The parameters are the components on the unstable (6-d) and neutral (4-d) linear spaces. The only condition on the stable component is that it is small enough.

The main technical point is to show that the coefficients of the unstable and neutral eigenfunctions do not grow, and in fact decrease as $p \to p+1$.

The main technical point is to show that the coefficients of the unstable and neutral eigenfunctions do not grow, and in fact decrease as $p \to p+1$.

The proof is based on renormalization group methods. The function $\Lambda(s)$ turns out to be differentiable and strictly increasing.

The main technical point is to show that the coefficients of the unstable and neutral eigenfunctions do not grow, and in fact decrease as $p \to p+1$.

The proof is based on renormalization group methods. The function $\Lambda(s)$ turns out to be differentiable and strictly increasing. Establishing the properties of $\Lambda(s)$ is an important technical point, to which some separate papers were devoted.

The main technical point is to show that the coefficients of the unstable and neutral eigenfunctions do not grow, and in fact decrease as $p \to p+1$.

The proof is based on renormalization group methods. The function $\Lambda(s)$ turns out to be differentiable and strictly increasing. Establishing the properties of $\Lambda(s)$ is an important technical point, to which some separate papers were devoted.

The finite time blow-up follows immediatedly from the fundamental Ansatz. We have

$$A^p \mathbf{h}^{(p)}(\mathbf{Y}, t) = p(A\Lambda(t))^p g^{(3)}(\mathbf{Y}) \left(\mathbf{H}^{(0)}(\mathbf{Y}) + \delta^{(p)}(\mathbf{Y}, t) \right).$$

As Λ is strictly increasing, the power series diverges at $t = \tau$ if $|A| = \frac{1}{\Lambda(\tau)}$.

The solutions are complex-valued,

The solutions are complex-valued, and both energy and enstrophy diverge as $t \uparrow \tau$ as inverse powers of $\tau - t$.

The solutions are complex-valued, and both energy and enstrophy diverge as $t \uparrow \tau$ as inverse powers of $\tau - t$.

Two types of solutions. The recursive equations for $\mathbf{h}^{(p)}$ are unchanged if we replace $\mathbf{h}^{(p)}$ with $(-1)^p \mathbf{h}^{(p)}$.

The solutions are complex-valued, and both energy and enstrophy diverge as $t \uparrow \tau$ as inverse powers of $\tau - t$.

Two types of solutions. The recursive equations for $\mathbf{h}^{(p)}$ are unchanged if we replace $\mathbf{h}^{(p)}$ with $(-1)^p \mathbf{h}^{(p)}$. Hence we have two types of solutions, corresponding to positive and negative A.

The solutions are complex-valued, and both energy and enstrophy diverge as $t \uparrow \tau$ as inverse powers of $\tau - t$.

Two types of solutions. The recursive equations for $\mathbf{h}^{(p)}$ are unchanged if we replace $\mathbf{h}^{(p)}$ with $(-1)^p \mathbf{h}^{(p)}$. Hence we have two types of solutions, corresponding to positive and negative A. The total energy $E(t)$ and the total enstrophy blow up with different power laws in $\tau - t$

The solutions are complex-valued, and both energy and enstrophy diverge as $t \uparrow \tau$ as inverse powers of $\tau - t$.

Two types of solutions. The recursive equations for $\mathbf{h}^{(p)}$ are unchanged if we replace $\mathbf{h}^{(p)}$ with $(-1)^p \mathbf{h}^{(p)}$. Hence we have two types of solutions, corresponding to positive and negative A. The total energy $E(t)$ and the total enstrophy blow up with different power laws in $\tau - t$

$$E(t) = \frac{(2\pi)^3}{2} \int_{\mathbb{R}^3} |\mathbf{v}(\mathbf{k}, t)|^2 d\mathbf{k}, \sim \frac{C_E^{(\alpha)}}{(\tau - t)^{\beta_\alpha}},$$

$$S(t) = (2\pi)^3 \int_{\mathbb{R}^3} \mathbf{k}^2 |\mathbf{v}(\mathbf{k}, t)|^2 d\mathbf{k} \sim \frac{C_S^{(\alpha)}}{(\tau - t)^{\beta_\alpha + 2}},$$

The solutions are complex-valued, and both energy and enstrophy diverge as $t \uparrow \tau$ as inverse powers of $\tau - t$.

Two types of solutions. The recursive equations for $\mathbf{h}^{(p)}$ are unchanged if we replace $\mathbf{h}^{(p)}$ with $(-1)^p \mathbf{h}^{(p)}$. Hence we have two types of solutions, corresponding to positive and negative A. The total energy $E(t)$ and the total enstrophy blow up with different power laws in $\tau - t$

$$E(t) = \frac{(2\pi)^3}{2} \int_{\mathbb{R}^3} |\mathbf{v}(\mathbf{k}, t)|^2 d\mathbf{k}, \sim \frac{C_E^{(\alpha)}}{(\tau - t)^{\beta_\alpha}},$$

$$S(t) = (2\pi)^3 \int_{\mathbb{R}^3} \mathbf{k}^2 |\mathbf{v}(\mathbf{k}, t)|^2 d\mathbf{k} \sim \frac{C_S^{(\alpha)}}{(\tau - t)^{\beta_\alpha + 2}},$$

where $\beta_+ = 1$, $\beta_- = \frac{1}{2}$, $C_E^{(\alpha)}$, $C_S^{(\alpha)}$ are constants, and $\alpha = \pm$ is the sign of A.

The singular solutions of Li and Sinai have the following properties (*C.B., S.Frigio & P. Maponi 2017*) :

The singular solutions of Li and Sinai have the following properties (*C.B., S.Frigio & P. Maponi 2017*) :

i) The solution $\mathbf{v}(\mathbf{k}, t)$ is represented as a sum of modulated gaussian-dominated terms concentrated around the points $p\mathbf{k}^{(0)} = (0, 0, p\ a)$, multiplied by $\exp\{-\kappa(t)\ p(\tau - t)\}$ (coming from $(A\Lambda(t))^p$).

The singular solutions of Li and Sinai have the following properties (*C.B., S.Frigio & P. Maponi 2017*) :

i) The solution $\mathbf{v}(\mathbf{k}, t)$ is represented as a sum of modulated gaussian-dominated terms concentrated around the points $p\mathbf{k}^{(0)} = (0, 0, p\ a)$, multiplied by $\exp\{-\kappa(t)\ p(\tau - t)\}$ (coming from $(A\Lambda(t))^p$). Hence its main support is within a thin cone along the k_3-axis;

The singular solutions of Li and Sinai have the following properties (*C.B., S.Frigio & P. Maponi 2017*) :

i) The solution $\mathbf{v}(\mathbf{k}, t)$ is represented as a sum of modulated gaussian-dominated terms concentrated around the points $p\mathbf{k}^{(0)} = (0, 0, p\ a)$, multiplied by $\exp\{-\kappa(t)\ p(\tau - t)\}$ (coming from $(A\Lambda(t))^p$). Hence its main support is within a thin cone along the k_3-axis;

ii) For large k_3, the velocity field is approximately orthogonal to the k_3-axis and aligned to the fixed point $\mathbf{H}^{(0)}$;

The singular solutions of Li and Sinai have the following properties (*C.B., S.Frigio & P. Maponi 2017*) :

i) The solution $\mathbf{v}(\mathbf{k}, t)$ is represented as a sum of modulated gaussian-dominated terms concentrated around the points $p\mathbf{k}^{(0)} = (0, 0, p\ a)$, multiplied by $\exp\{-\kappa(t)\ p(\tau - t)\}$ (coming from $(A\Lambda(t))^p$). Hence its main support is within a thin cone along the k_3-axis;

ii) For large k_3, the velocity field is approximately orthogonal to the k_3-axis and aligned to the fixed point $\mathbf{H}^{(0)}$;

iii) The solutions converge point-wise in $\mathbf{k}$-space as $t \uparrow \tau$,

The singular solutions of Li and Sinai have the following properties (*C.B., S.Frigio & P. Maponi 2017*) :

i) The solution $\mathbf{v}(\mathbf{k}, t)$ is represented as a sum of modulated gaussian-dominated terms concentrated around the points $p\mathbf{k}^{(0)} = (0, 0, p\ a)$, multiplied by $\exp\{-\kappa(t)\ p(\tau - t)\}$ (coming from $(A\Lambda(t))^p$). Hence its main support is within a thin cone along the k_3-axis;

ii) For large k_3, the velocity field is approximately orthogonal to the k_3-axis and aligned to the fixed point $\mathbf{H}^{(0)}$;

iii) The solutions converge point-wise in $\mathbf{k}$-space as $t \uparrow \tau$, while $E(t)$ and $S(t)$ diverge as inverse powers of $\tau - t$, depending on the sign of A.

The singular solutions of Li and Sinai have the following properties (*C.B., S.Frigio & P. Maponi 2017*) :

i) The solution $\mathbf{v}(\mathbf{k}, t)$ is represented as a sum of modulated gaussian-dominated terms concentrated around the points $p\mathbf{k}^{(0)} = (0, 0, p\ a)$, multiplied by $\exp\{-\kappa(t)\ p(\tau - t)\}$ (coming from $(A\Lambda(t))^p$). Hence its main support is within a thin cone along the k_3-axis;

ii) For large k_3, the velocity field is approximately orthogonal to the k_3-axis and aligned to the fixed point $\mathbf{H}^{(0)}$;

iii) The solutions converge point-wise in $\mathbf{k}$-space as $t \uparrow \tau$, while $E(t)$ and $S(t)$ diverge as inverse powers of $\tau - t$, depending on the sign of A.

For a better understanding of the behavior of the solutions, also in view of extending the analysis to the associated real solutions, we resorted to computer simulations.

3. LI-SINAI SOLUTIONS. SIMULATIONS

The computer simulations for the complex Li-Sinai solutions reveal important properties which the theory cannot easily predict.

3. LI-SINAI SOLUTIONS. SIMULATIONS

The computer simulations for the complex Li-Sinai solutions reveal important properties which the theory cannot easily predict. They can also be extended, as shown in what follows, to the case of related real solutions, for which there are few theoretical results.

3. LI-SINAI SOLUTIONS. SIMULATIONS

The computer simulations for the complex Li-Sinai solutions reveal important properties which the theory cannot easily predict. They can also be extended, as shown in what follows, to the case of related real solutions, for which there are few theoretical results.

The simulations were performed first at the Fermi and later at the Marconi Supercomputers of CINECA (Bologna, Italy), using a special program for solutions of the integral equation in **k**-space.

3. LI-SINAI SOLUTIONS. SIMULATIONS

The computer simulations for the complex Li-Sinai solutions reveal important properties which the theory cannot easily predict. They can also be extended, as shown in what follows, to the case of related real solutions, for which there are few theoretical results.

The simulations were performed first at the Fermi and later at the Marconi Supercomputers of CINECA (Bologna, Italy), using a special program for solutions of the integral equation in **k**-space. A similar program was previously used for simulating the blow-up of complex solutions of the 2-d Burgers equation.

3. LI-SINAI SOLUTIONS. SIMULATIONS

The computer simulations for the complex Li-Sinai solutions reveal important properties which the theory cannot easily predict. They can also be extended, as shown in what follows, to the case of related real solutions, for which there are few theoretical results.

The simulations were performed first at the Fermi and later at the Marconi Supercomputers of CINECA (Bologna, Italy), using a special program for solutions of the integral equation in $\mathbf{k}$-space. A similar program was previously used for simulating the blow-up of complex solutions of the 2-d Burgers equation.

The blow-up is best followed by looking at the behavior of the total enstrophy $S(t)$, which describes the flow of energy to the microscale in the physical space, and of its marginals in $\mathbf{k}$-space.

The initial data for the complex solutions prescribed by Li and Sinai are of the type $\mathbf{v}_0^{\pm} = \pm K\, \bar{\mathbf{v}}_0(\mathbf{k})$, $K > 0$ with

$$\bar{\mathbf{v}}_0(\mathbf{k}) = \left(k_1, k_2, -\frac{k_1^2 + k_2^2}{k_3} + \Phi(\mathbf{k}) \right) g^{(3)}(\mathbf{k} - \mathbf{k}^{(0)}) \chi_b(k_3 - a),$$

The initial data for the complex solutions prescribed by Li and Sinai are of the type $\mathbf{v}_0^{\pm} = \pm K\, \bar{\mathbf{v}}_0(\mathbf{k})$, $K > 0$ with

$$\bar{\mathbf{v}}_0(\mathbf{k}) = \left(k_1, k_2, -\frac{k_1^2 + k_2^2}{k_3} + \Phi(\mathbf{k}) \right) g^{(3)}(\mathbf{k} - \mathbf{k}^{(0)}) \chi_b(k_3 - a),$$

where $\mathbf{k}^{(0)} = (0, 0, a)$, $a > b > 0$ and $\chi_b(x)$ is a smooth function such that $\chi_b(x) = 0, |x| > b$, $\chi_b(x) = 1, |x| < b - \epsilon$, $\epsilon << b$ is a cutoff to avoid the singularity at $k_3 = 0$.

The initial data for the complex solutions prescribed by Li and Sinai are of the type $\mathbf{v}_0^{\pm} = \pm K\ \bar{\mathbf{v}}_0(\mathbf{k})$, $K > 0$ with

$$\bar{\mathbf{v}}_0(\mathbf{k}) = \left(k_1, k_2, -\frac{k_1^2 + k_2^2}{k_3} + \Phi(\mathbf{k}) \right) g^{(3)}(\mathbf{k} - \mathbf{k}^{(0)}) \chi_b(k_3 - a),$$

where $\mathbf{k}^{(0)} = (0, 0, a)$, $a > b > 0$ and $\chi_b(x)$ is a smooth function such that $\chi_b(x) = 0, |x| > b$, $\chi_b(x) = 1, |x| < b - \epsilon$, $\epsilon << b$ is a cutoff to avoid the singularity at $k_3 = 0$.
We denote by $\mathbf{v}^{\pm}(\mathbf{k}, t)$ the solutions with initial data $\mathbf{v}_0^{\pm}$. K controls the initial energy.

The initial data for the complex solutions prescribed by Li and Sinai are of the type $\mathbf{v}_0^{\pm} = \pm K\, \bar{\mathbf{v}}_0(\mathbf{k})$, $K > 0$ with

$$\bar{\mathbf{v}}_0(\mathbf{k}) = \left(k_1, k_2, -\frac{k_1^2 + k_2^2}{k_3} + \Phi(\mathbf{k}) \right) g^{(3)}(\mathbf{k} - \mathbf{k}^{(0)}) \chi_b(k_3 - a),$$

where $\mathbf{k}^{(0)} = (0, 0, a)$, $a > b > 0$ and $\chi_b(x)$ is a smooth function such that $\chi_b(x) = 0, |x| > b$, $\chi_b(x) = 1, |x| < b - \epsilon$, $\epsilon << b$ is a cutoff to avoid the singularity at $k_3 = 0$.
We denote by $\mathbf{v}^{\pm}(\mathbf{k}, t)$ the solutions with initial data $\mathbf{v}_0^{\pm}$. K controls the initial energy.

The function Φ is a linear combination of the eigenfunctions of the linearization of the renormalization group map.

The initial data for the complex solutions prescribed by Li and Sinai are of the type $\mathbf{v}_0^{\pm} = \pm K\, \bar{\mathbf{v}}_0(\mathbf{k})$, $K > 0$ with

$$\bar{\mathbf{v}}_0(\mathbf{k}) = \left(k_1, k_2, -\frac{k_1^2 + k_2^2}{k_3} + \Phi(\mathbf{k}) \right) g^{(3)}(\mathbf{k} - \mathbf{k}^{(0)}) \chi_b(k_3 - a),$$

where $\mathbf{k}^{(0)} = (0, 0, a)$, $a > b > 0$ and $\chi_b(x)$ is a smooth function such that $\chi_b(x) = 0, |x| > b$, $\chi_b(x) = 1, |x| < b - \epsilon$, $\epsilon << b$ is a cutoff to avoid the singularity at $k_3 = 0$.
We denote by $\mathbf{v}^{\pm}(\mathbf{k}, t)$ the solutions with initial data $\mathbf{v}_0^{\pm}$. K controls the initial energy.

The function Φ is a linear combination of the eigenfunctions of the linearization of the renormalization group map. The simulations show that it does not play a significant role in the evolution, except perhaps it slows down the blow up,

The initial data for the complex solutions prescribed by Li and Sinai are of the type $\mathbf{v}_0^{\pm} = \pm K\, \bar{\mathbf{v}}_0(\mathbf{k})$, $K > 0$ with

$$\bar{\mathbf{v}}_0(\mathbf{k}) = \left(k_1, k_2, -\frac{k_1^2 + k_2^2}{k_3} + \Phi(\mathbf{k}) \right) g^{(3)}(\mathbf{k} - \mathbf{k}^{(0)}) \chi_b(k_3 - a),$$

where $\mathbf{k}^{(0)} = (0, 0, a)$, $a > b > 0$ and $\chi_b(x)$ is a smooth function such that $\chi_b(x) = 0, |x| > b$, $\chi_b(x) = 1, |x| < b - \epsilon$, $\epsilon << b$ is a cutoff to avoid the singularity at $k_3 = 0$.
We denote by $\mathbf{v}^{\pm}(\mathbf{k}, t)$ the solutions with initial data $\mathbf{v}_0^{\pm}$. K controls the initial energy.

The function Φ is a linear combination of the eigenfunctions of the linearization of the renormalization group map. The simulations show that it does not play a significant role in the evolution, except perhaps it slows down the blow up, so as a rule we took $\Phi = 0$.

Our mesh in $\mathbf{k}$-space is a regular lattice containing the origin with step, in most cases, $\delta = 1$, i.e., a subset of $\mathbb{Z}^3$.

Our mesh in $\mathbf{k}$-space is a regular lattice containing the origin with step, in most cases, $\delta = 1$, i.e., a subset of $\mathbb{Z}^3$. As the support is concentrated in a thin cone around the positive k_3-axis, we can follow the solutions for values of $|\mathbf{k}|$ in the range of a few thousand.

Our mesh in $\mathbf{k}$-space is a regular lattice containing the origin with step, in most cases, $\delta = 1$, i.e., a subset of $\mathbb{Z}^3$. As the support is concentrated in a thin cone around the positive k_3-axis, we can follow the solutions for values of $|\mathbf{k}|$ in the range of a few thousand.

The maximal configuration of our mesh was $[-254, 254]^2 \times$ $\times [-20, 4000]$.

Our mesh in $\mathbf{k}$-space is a regular lattice containing the origin with step, in most cases, $\delta = 1$, i.e., a subset of $\mathbb{Z}^3$. As the support is concentrated in a thin cone around the positive k_3-axis, we can follow the solutions for values of $|\mathbf{k}|$ in the range of a few thousand.

The maximal configuration of our mesh was $[-254, 254]^2 \times$ $\times [-20, 4000]$. The field is represented by an array of about $3 \cdot 10^9$ real numbers, close to the maximal capacity of modern supercomputers.

Our mesh in $\mathbf{k}$-space is a regular lattice containing the origin with step, in most cases, $\delta = 1$, i.e., a subset of $\mathbb{Z}^3$. As the support is concentrated in a thin cone around the positive k_3-axis, we can follow the solutions for values of $|\mathbf{k}|$ in the range of a few thousand.

The maximal configuration of our mesh was $[-254, 254]^2 \times$ $\times [-20, 4000]$. The field is represented by an array of about $3 \cdot 10^9$ real numbers, close to the maximal capacity of modern supercomputers.

The total enstrophy and its marginals, which depend on the behavior for large $|\mathbf{k}|$, are stable with respect to a refinement of the mesh.

Our mesh in $\mathbf{k}$-space is a regular lattice containing the origin with step, in most cases, $\delta = 1$, i.e., a subset of $\mathbb{Z}^3$. As the support is concentrated in a thin cone around the positive k_3-axis, we can follow the solutions for values of $|\mathbf{k}|$ in the range of a few thousand.

The maximal configuration of our mesh was $[-254, 254]^2 \times$ $\times [-20, 4000]$. The field is represented by an array of about $3 \cdot 10^9$ real numbers, close to the maximal capacity of modern supercomputers.

The total enstrophy and its marginals, which depend on the behavior for large $|\mathbf{k}|$, are stable with respect to a refinement of the mesh. But, as the diameter of the support of $\mathbf{v}_0$ is $\mathcal{O}(1)$, the step $\delta = 1$ does not allow a accuracy for the large and medium size features in $\mathbf{x}$-space.

Our mesh in $\mathbf{k}$-space is a regular lattice containing the origin with step, in most cases, $\delta = 1$, i.e., a subset of $\mathbb{Z}^3$. As the support is concentrated in a thin cone around the positive k_3-axis, we can follow the solutions for values of $|\mathbf{k}|$ in the range of a few thousand.

The maximal configuration of our mesh was $[-254, 254]^2 \times$ $\times [-20, 4000]$. The field is represented by an array of about $3 \cdot 10^9$ real numbers, close to the maximal capacity of modern supercomputers.

The total enstrophy and its marginals, which depend on the behavior for large $|\mathbf{k}|$, are stable with respect to a refinement of the mesh. But, as the diameter of the support of $\mathbf{v}_0$ is $\mathcal{O}(1)$, the step $\delta = 1$ does not allow a accuracy for the large and medium size features in $\mathbf{x}$-space. A comparison of our computation methods with the modern difference schemes is under way.

For values $a \geq 20$ and initial energy E_0 large enough, of the order $\mathcal{O}(10^5)$ or more, the solutions blow up, and can be followed up to times close to the critical blow-up time.

For values $a \geq 20$ and initial energy E_0 large enough, of the order $\mathcal{O}(10^5)$ or more, the solutions blow up, and can be followed up to times close to the critical blow-up time.

The blow-up takes place in a very short time, of the order of $10^{-4} - 10^{-3}$ time units with a time mesh of step of the order $10^{-7} - 10^{-8}$.

For values $a \geq 20$ and initial energy E_0 large enough, of the order $\mathcal{O}(10^5)$ or more, the solutions blow up, and can be followed up to times close to the critical blow-up time.

The blow-up takes place in a very short time, of the order of $10^{-4} - 10^{-3}$ time units with a time mesh of step of the order $10^{-7} - 10^{-8}$.

It is possible that for smaller values of a and E_0 there is also a blow-up,

For values $a \geq 20$ and initial energy E_0 large enough, of the order $\mathcal{O}(10^5)$ or more, the solutions blow up, and can be followed up to times close to the critical blow-up time.

The blow-up takes place in a very short time, of the order of $10^{-4} - 10^{-3}$ time units with a time mesh of step of the order $10^{-7} - 10^{-8}$.

It is possible that for smaller values of a and E_0 there is also a blow-up, but, if so, it takes a longer computer time than what is available.

For values $a \geq 20$ and initial energy E_0 large enough, of the order $\mathcal{O}(10^5)$ or more, the solutions blow up, and can be followed up to times close to the critical blow-up time.

The blow-up takes place in a very short time, of the order of $10^{-4} - 10^{-3}$ time units with a time mesh of step of the order $10^{-7} - 10^{-8}$.

It is possible that for smaller values of a and E_0 there is also a blow-up, but, if so, it takes a longer computer time than what is available.

The simulations were carried out within the framework of a European PRACE Project n. 2015133169, and also of CINECA ISCRA Projects of type B and C.

The solutions "stays quiet" for about 10^{-3} t.u., with energy and enstrophy decreasing,

The solutions "stays quiet" for about 10^{-3} t.u., with energy and enstrophy decreasing, then both quantities increase rapidly, leading to a blow-up in a time of the order 10^{-5}.

The solutions "stays quiet" for about 10^{-3} t.u., with energy and enstrophy decreasing, then both quantities increase rapidly, leading to a blow-up in a time of the order 10^{-5}.

Most simulations were done for solutions of type $\mathbf{v}^-$.

The solutions "stays quiet" for about 10^{-3} t.u., with energy and enstrophy decreasing, then both quantities increase rapidly, leading to a blow-up in a time of the order 10^{-5}.

Most simulations were done for solutions of type $\mathbf{v}^-$. Their behavior is more similar to that of the related real solutions.

The solutions "stays quiet" for about 10^{-3} t.u., with energy and enstrophy decreasing, then both quantities increase rapidly, leading to a blow-up in a time of the order 10^{-5}.

Most simulations were done for solutions of type $\mathbf{v}^-$. Their behavior is more similar to that of the related real solutions.

For the description of the blow-up we consider the total energy and enstrophy and the correspondent marginals in $\mathbf{k}$-space along the main axes

$$E_3(k_3, t) = \frac{1}{2} \int_{\mathbb{R}\times\mathbb{R}} dk_1 dk_2 |\mathbf{v}(\mathbf{k}, t)|^2,$$

$$S_3(k_3, t) = \int_{\mathbb{R}\times\mathbb{R}} dk_1 dk_2 |\mathbf{k}|^2 |\mathbf{v}(\mathbf{k}, t)|^2$$

The solutions "stays quiet" for about 10^{-3} t.u., with energy and enstrophy decreasing, then both quantities increase rapidly, leading to a blow-up in a time of the order 10^{-5}.

Most simulations were done for solutions of type $\mathbf{v}^-$. Their behavior is more similar to that of the related real solutions.

For the description of the blow-up we consider the total energy and enstrophy and the correspondent marginals in $\mathbf{k}$-space along the main axes

$$E_3(k_3,t) = \frac{1}{2}\int_{\mathbb{R}\times\mathbb{R}} dk_1 dk_2 |\mathbf{v}(\mathbf{k},t)|^2,$$

$$S_3(k_3,t) = \int_{\mathbb{R}\times\mathbb{R}} dk_1 dk_2 |\mathbf{k}|^2 |\mathbf{v}(\mathbf{k},t)|^2$$

and the analogous marginals $E_j(k_j,t)$, $S_j(k_j,t)$, $j=1,2$.

We show some pictures obtained by computer simulations which illustrate two main features of the blow-up in **k**-space, qualitatively predicted by the theory:

We show some pictures obtained by computer simulations which illustrate two main features of the blow-up in $\mathbf{k}$-space, qualitatively predicted by the theory:

i) The support is concentrated in regions centered around the points $p\mathbf{k}^{(0)} = (0, 0, pa)$, $p = 1, 2, \ldots$ with significant diameter $\mathcal{O}(\sqrt{p})$,

We show some pictures obtained by computer simulations which illustrate two main features of the blow-up in $\mathbf{k}$-space, qualitatively predicted by the theory:

i) The support is concentrated in regions centered around the points $p\mathbf{k}^{(0)} = (0, 0, pa)$, $p = 1, 2, \ldots$ with significant diameter $\mathcal{O}(\sqrt{p})$, and well separated as long as $p < a^2$.

We show some pictures obtained by computer simulations which illustrate two main features of the blow-up in $\mathbf{k}$-space, qualitatively predicted by the theory:

i) The support is concentrated in regions centered around the points $p\mathbf{k}^{(0)} = (0, 0, pa)$, $p = 1, 2, \ldots$ with significant diameter $\mathcal{O}(\sqrt{p})$, and well separated as long as $p < a^2$.

ii) The marginals $E_3(k_3, t)$ and $S_3(k_3, t)$ show sharp oscillations with maxima at the points $p\mathbf{k}^{(0)}$,

We show some pictures obtained by computer simulations which illustrate two main features of the blow-up in $\mathbf{k}$-space, qualitatively predicted by the theory:

i) The support is concentrated in regions centered around the points $p\mathbf{k}^{(0)} = (0, 0, pa)$, $p = 1, 2, \ldots$ with significant diameter $\mathcal{O}(\sqrt{p})$, and well separated as long as $p < a^2$.

ii) The marginals $E_3(k_3, t)$ and $S_3(k_3, t)$ show sharp oscillations with maxima at the points $p\mathbf{k}^{(0)}$, modulated by an exponential $\exp\{-\kappa(t)k_3\}$, where, if t_c is the critical time,

$$\kappa(t) = \alpha(t_c - t), \qquad \alpha = \frac{\Lambda'(t_c)}{a\,\Lambda(t_c)}.$$

We show some pictures obtained by computer simulations which illustrate two main features of the blow-up in $\mathbf{k}$-space, qualitatively predicted by the theory:

i) The support is concentrated in regions centered around the points $p\mathbf{k}^{(0)} = (0, 0, pa)$, $p = 1, 2, \ldots$ with significant diameter $\mathcal{O}(\sqrt{p})$, and well separated as long as $p < a^2$.

ii) The marginals $E_3(k_3, t)$ and $S_3(k_3, t)$ show sharp oscillations with maxima at the points $p\mathbf{k}^{(0)}$, modulated by an exponential $\exp\{-\kappa(t)k_3\}$, where, if t_c is the critical time,

$$\kappa(t) = \alpha(t_c - t), \qquad \alpha = \frac{\Lambda'(t_c)}{a\,\Lambda(t_c)}.$$

The behavior of the exponential decay rate allows a good estimate of the critical time t_c.

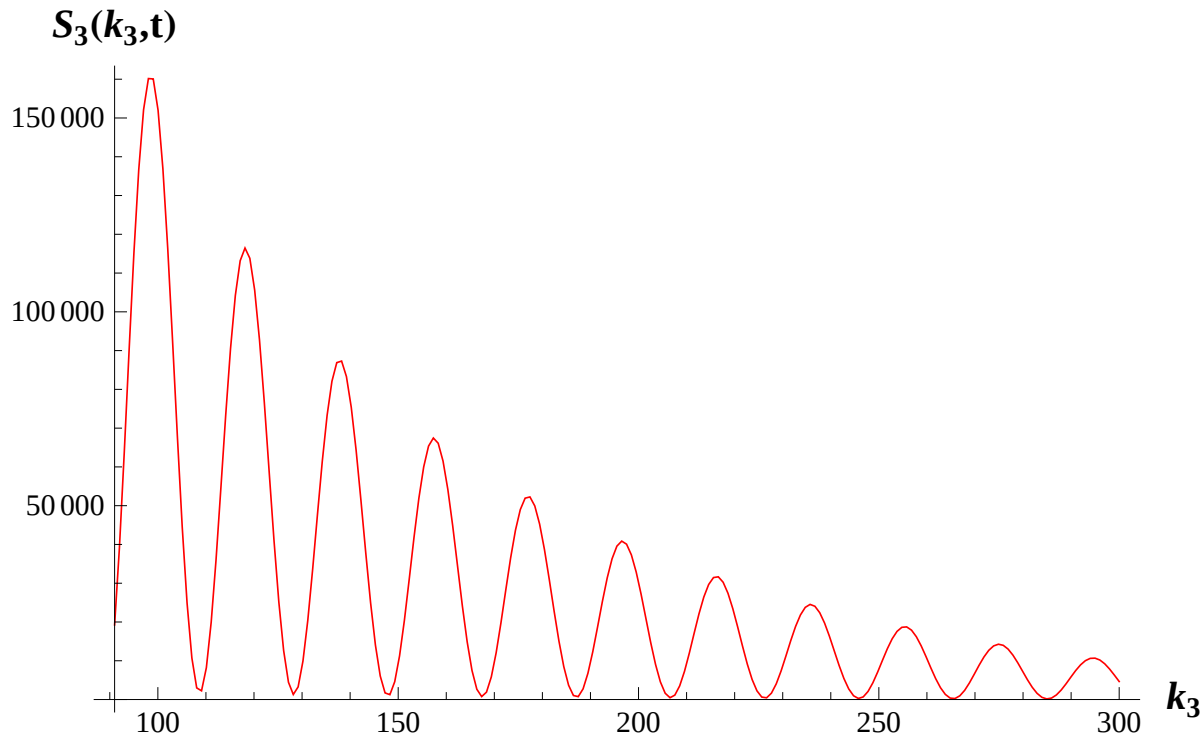

Figure 1: $a = 20$, $E_0 = 5 \times 10^4$. *Enstrophy marginal density* $S_3(k_3, t)$ *at* $t = 1125 \times 10^{-7}$. *The zeroes are approximately periodic with period* a. *Simulation range* $k_3 \in [-19, 2528]$.

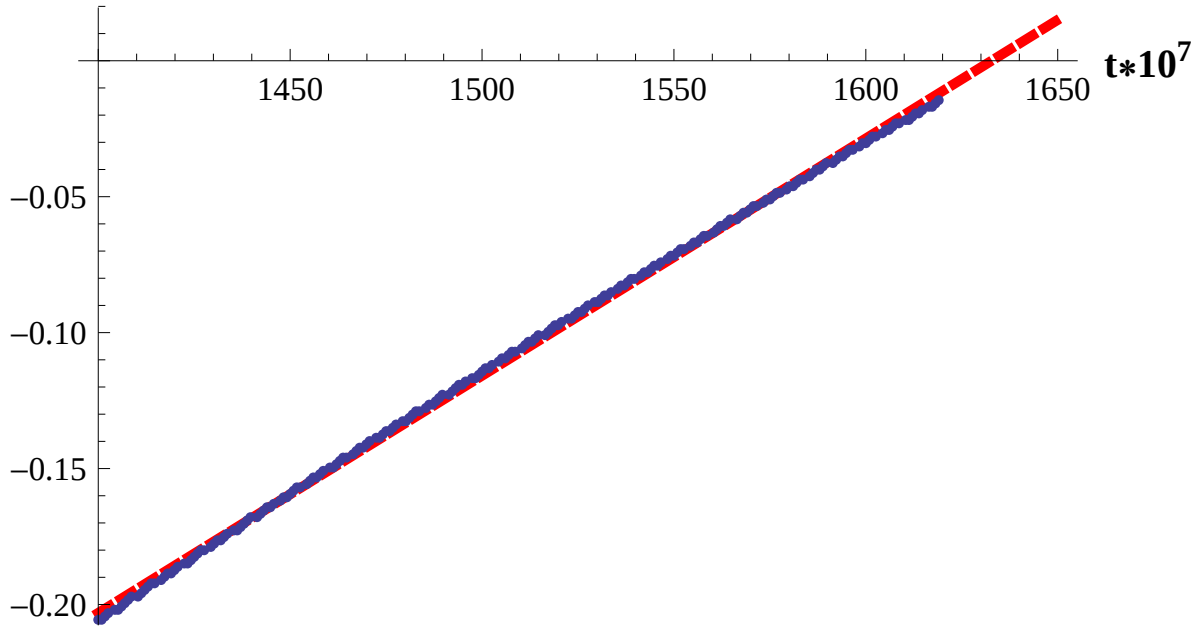

Figure 2: $a = 20$, $E_0 = 5 \times 10^4$. *Exponential decay rate* $-\kappa(t)$ *for the marginal density* $E_3(k_3, t)$, *taken for* $k_3 \geq 400$, *vs magnified time* $t \times 10^7$, *with linear regression (dashed line). Simulation range* $k_3 \in [-19, 2528]$.

4. REAL ANTISYMMETRIC SOLUTIONS. INTRODUCTION

In the search for the GRP, it is natural to consider the real flows obtained by antisymmetrizing the initial data of the complex solutions that blow-up.

4. REAL ANTISYMMETRIC SOLUTIONS. INTRODUCTION

In the search for the GRP, it is natural to consider the real flows obtained by antisymmetrizing the initial data of the complex solutions that blow-up.

The support of the initial data is now essentially contained in two finite regions around the points $\pm\mathbf{k}^{(0)}$.

4. REAL ANTISYMMETRIC SOLUTIONS. INTRODUCTION

In the search for the GRP, it is natural to consider the real flows obtained by antisymmetrizing the initial data of the complex solutions that blow-up.

The support of the initial data is now essentially contained in two finite regions around the points $\pm\mathbf{k}^{(0)}$.The convolutions $\mathbf{g}^{(p)}$ are no more centered around the point $p\mathbf{k}^{(0)} = (0, 0, pa)$, but are sums of contributions centered around the points $(0, 0, \ell a)$ with $\ell = -p, \ldots, p$.

4. REAL ANTISYMMETRIC SOLUTIONS. INTRODUCTION

In the search for the GRP, it is natural to consider the real flows obtained by antisymmetrizing the initial data of the complex solutions that blow-up.

The support of the initial data is now essentially contained in two finite regions around the points $\pm\mathbf{k}^{(0)}$.The convolutions $\mathbf{g}^{(p)}$ are no more centered around the point $p\mathbf{k}^{(0)} = (0, 0, pa)$, but are sums of contributions centered around the points $(0, 0, \ell a)$ with $\ell = -p, \ldots, p$. The main contribution comes for $|\ell| = \mathcal{O}(\sqrt{p})$.

4. REAL ANTISYMMETRIC SOLUTIONS. INTRODUCTION

In the search for the GRP, it is natural to consider the real flows obtained by antisymmetrizing the initial data of the complex solutions that blow-up.

The support of the initial data is now essentially contained in two finite regions around the points $\pm\mathbf{k}^{(0)}$.The convolutions $\mathbf{g}^{(p)}$ are no more centered around the point $p\mathbf{k}^{(0)} = (0, 0, pa)$, but are sums of contributions centered around the points $(0, 0, \ell a)$ with $\ell = -p, \ldots, p$. The main contribution comes for $|\ell| = \mathcal{O}(\sqrt{p})$.

Therefore, by the convolution mechanism, when the components $\mathbf{g}^{(p)}$ for large p are excited, the support moves to the high $\mathbf{k}$ region.

4. REAL ANTISYMMETRIC SOLUTIONS. INTRODUCTION

In the search for the GRP, it is natural to consider the real flows obtained by antisymmetrizing the initial data of the complex solutions that blow-up.

The support of the initial data is now essentially contained in two finite regions around the points $\pm\mathbf{k}^{(0)}$.The convolutions $\mathbf{g}^{(p)}$ are no more centered around the point $p\mathbf{k}^{(0)} = (0, 0, pa)$, but are sums of contributions centered around the points $(0, 0, \ell a)$ with $\ell = -p, \ldots, p$. The main contribution comes for $|\ell| = \mathcal{O}(\sqrt{p})$.

Therefore, by the convolution mechanism, when the components $\mathbf{g}^{(p)}$ for large p are excited, the support moves to the high $\mathbf{k}$ region. The mechanism is not as "good" as for the complex case, but it is rather efficient, especially if a is large.

In spite of the restrictions, the set of the real solutions related to complex solutions that bow-up is very large.

In spite of the restrictions, the set of the real solutions related to complex solutions that bow-up is very large. In fact we expect that the results on the blow-up can be extended to other fixed points $\mathbf{H} \neq \mathbf{H}^{(0)}$.

In spite of the restrictions, the set of the real solutions related to complex solutions that bow-up is very large. In fact we expect that the results on the blow-up can be extended to other fixed points $\mathbf{H} \neq \mathbf{H}^{(0)}$. Li and Sinai prove that there are infinitely many fixed points, which can be written down explicitly.

In spite of the restrictions, the set of the real solutions related to complex solutions that bow-up is very large. In fact we expect that the results on the blow-up can be extended to other fixed points $\mathbf{H} \neq \mathbf{H}^{(0)}$. Li and Sinai prove that there are infinitely many fixed points, which can be written down explicitly.

We can define classes of real NS flows, labeled by the fixed points $\mathbf{H}$. The solutions of each class follow from initial data obtained by antisymmetrizing initial data leading to a complex blow-up with a given fixed point.

In spite of the restrictions, the set of the real solutions related to complex solutions that bow-up is very large. In fact we expect that the results on the blow-up can be extended to other fixed points $\mathbf{H} \neq \mathbf{H}^{(0)}$. Li and Sinai prove that there are infinitely many fixed points, which can be written down explicitly.

We can define classes of real NS flows, labeled by the fixed points $\mathbf{H}$. The solutions of each class follow from initial data obtained by antisymmetrizing initial data leading to a complex blow-up with a given fixed point.

The theoretical analysis requires the extension of the blow-up analysis to other fixed points,

In spite of the restrictions, the set of the real solutions related to complex solutions that bow-up is very large. In fact we expect that the results on the blow-up can be extended to other fixed points $\mathbf{H} \neq \mathbf{H}^{(0)}$. Li and Sinai prove that there are infinitely many fixed points, which can be written down explicitly.

We can define classes of real NS flows, labeled by the fixed points $\mathbf{H}$. The solutions of each class follow from initial data obtained by antisymmetrizing initial data leading to a complex blow-up with a given fixed point.

The theoretical analysis requires the extension of the blow-up analysis to other fixed points, and an adequate understanding of the behavior of the functions $\mathbf{g}^{(p)}$ for the new real solutions.

In the meantime important information can be obtained by computer simulations, which can also reveal physically relevant details.

In the meantime important information can be obtained by computer simulations, which can also reveal physically relevant details.

As a first step we report results of computer simulations obtained by antisymmetrizing the initial data leading to the blow-up with fixed point $\mathbf{H}^{(0)}$, i.e., with initial data

In the meantime important information can be obtained by computer simulations, which can also reveal physically relevant details.

As a first step we report results of computer simulations obtained by antisymmetrizing the initial data leading to the blow-up with fixed point $\mathbf{H}^{(0)}$, i.e., with initial data

$$\mathbf{v}_0(\mathbf{k}) = A\left(k_1, k_2, -\frac{k_1^2+k_2^2}{k_3}\right) g^{(2)}(\mathbf{k}^\perp)\times$$

$$\times\left[g(k_3-a)\chi_b(k_3-a)+g(k_3+a)\chi_b(k_3+a)\right].$$

Here $\mathbf{k}^\perp = (k_1, k_2)$, $g^{(r)}$ is the standard Gaussian in $\mathbb{R}^r$ ($g^{(1)} = g$), $\chi_b(x)$, with $b \in (\frac{a}{2}, a)$ is a smooth cutoff to avoid the singularity at $k_3 = 0$, and $A > 0$.

5. REAL ANTISYMMETRIC SOLUTIONS. SIMULATIONS

We report results of simulations with the following choice of the parameters:

5. REAL ANTISYMMETRIC SOLUTIONS. SIMULATIONS

We report results of simulations with the following choice of the parameters: $a = 30$ and A is such that the initial energy $E_0 = 2.5 \times 10^5$, in the range studied for the complex blow-up.

5. REAL ANTISYMMETRIC SOLUTIONS. SIMULATIONS

We report results of simulations with the following choice of the parameters: $a = 30$ and A is such that the initial energy $E_0 = 2.5 \times 10^5$, in the range studied for the complex blow-up.

Simulations for different values of a and A are under way.

5. REAL ANTISYMMETRIC SOLUTIONS. SIMULATIONS

We report results of simulations with the following choice of the parameters: $a = 30$ and A is such that the initial energy $E_0 = 2.5 \times 10^5$, in the range studied for the complex blow-up.

Simulations for different values of a and A are under way.

Recall however that the following scaling holds: If $\mathbf{v}(\mathbf{k}, t)$ is a solution with initial data $\mathbf{v}_0(\mathbf{k})$, and $\lambda > 0$ then

$$\mathbf{v}^{(\lambda)}(\mathbf{k}, t) = \lambda^2 \mathbf{v}(\lambda \mathbf{k}, \lambda^{-2} t)$$

is also a solution with initial data $\lambda^2 \mathbf{v}_0(\lambda \mathbf{k})$.

5. REAL ANTISYMMETRIC SOLUTIONS. SIMULATIONS

We report results of simulations with the following choice of the parameters: $a = 30$ and A is such that the initial energy $E_0 = 2.5 \times 10^5$, in the range studied for the complex blow-up.

Simulations for different values of a and A are under way.

Recall however that the following scaling holds: If $\mathbf{v}(\mathbf{k}, t)$ is a solution with initial data $\mathbf{v}_0(\mathbf{k})$, and $\lambda > 0$ then

$$\mathbf{v}^{(\lambda)}(\mathbf{k}, t) = \lambda^2 \mathbf{v}(\lambda \mathbf{k}, \lambda^{-2} t)$$

is also a solution with initial data $\lambda^2 \mathbf{v}_0(\lambda \mathbf{k})$.

As for the complex case, the mesh step is 1, with maximal configuration $[-254, 254] \times [-254, 254] \times [-3000, 3000]$.

5. REAL ANTISYMMETRIC SOLUTIONS. SIMULATIONS

We report results of simulations with the following choice of the parameters: $a = 30$ and A is such that the initial energy $E_0 = 2.5 \times 10^5$, in the range studied for the complex blow-up.

Simulations for different values of a and A are under way.

Recall however that the following scaling holds: If $\mathbf{v}(\mathbf{k}, t)$ is a solution with initial data $\mathbf{v}_0(\mathbf{k})$, and $\lambda > 0$ then

$$\mathbf{v}^{(\lambda)}(\mathbf{k}, t) = \lambda^2 \mathbf{v}(\lambda \mathbf{k}, \lambda^{-2} t)$$

is also a solution with initial data $\lambda^2 \mathbf{v}_0(\lambda \mathbf{k})$.

As for the complex case, the mesh step is 1, with maximal configuration $[-254, 254] \times [-254, 254] \times [-3000, 3000]$. With 3 components of $\mathbf{v}$ at each site, we deal with a set of $3 \times (508)^2 \times 6000 \approx 5 \times 10^9$ real numbers.

The slides that follow show the main features of the real solution resulting from the computer simulations.

The slides that follow show the main features of the real solution resulting from the computer simulations.

We give the plot of the marginal enstrophy distribution $S_3(k_3, t)$ at $t = 0$ and at $t = T_1 = 711\tau$, $\tau = 1.5625 \times 10^{-8}$,

The slides that follow show the main features of the real solution resulting from the computer simulations.

We give the plot of the marginal enstrophy distribution $S_3(k_3, t)$ at $t = 0$ and at $t = T_1 = 711\tau$, $\tau = 1.5625 \times 10^{-8}$, showing that the support moves to the high $|\mathbf{k}|$-region

The slides that follow show the main features of the real solution resulting from the computer simulations.

We give the plot of the marginal enstrophy distribution $S_3(k_3, t)$ at $t = 0$ and at $t = T_1 = 711\tau$, $\tau = 1.5625 \times 10^{-8}$, showing that the support moves to the high $|\mathbf{k}|$-region and concentrates around the points $p\mathbf{k}^{(0)} = = (0, 0, pa)$, $p = 0, \pm 1, \pm 2, \ldots$, with some overlapping.

The slides that follow show the main features of the real solution resulting from the computer simulations.

We give the plot of the marginal enstrophy distribution $S_3(k_3, t)$ at $t = 0$ and at $t = T_1 = 711\tau$, $\tau = 1.5625 \times 10^{-8}$, showing that the support moves to the high $|\mathbf{k}|$-region and concentrates around the points $p\mathbf{k}^{(0)} = = (0, 0, pa)$, $p = 0, \pm 1, \pm 2, \ldots$, with some overlapping.

There is actually a transition period, when only the $\mathbf{g}^{(p)}$ with low p are excited, and the support remains close to the origin.

The slides that follow show the main features of the real solution resulting from the computer simulations.

We give the plot of the marginal enstrophy distribution $S_3(k_3, t)$ at $t = 0$ and at $t = T_1 = 711\tau$, $\tau = 1.5625 \times 10^{-8}$, showing that the support moves to the high $|\mathbf{k}|$-region and concentrates around the points $p\mathbf{k}^{(0)} = = (0, 0, pa)$, $p = 0, \pm 1, \pm 2, \ldots$, with some overlapping.

There is actually a transition period, when only the $\mathbf{g}^{(p)}$ with low p are excited, and the support remains close to the origin.

The total enstrophy grows significantly,

The slides that follow show the main features of the real solution resulting from the computer simulations.

We give the plot of the marginal enstrophy distribution $S_3(k_3, t)$ at $t = 0$ and at $t = T_1 = 711\tau$, $\tau = 1.5625 \times 10^{-8}$, showing that the support moves to the high $|\mathbf{k}|$-region and concentrates around the points $p\mathbf{k}^{(0)} = = (0, 0, pa)$, $p = 0, \pm 1, \pm 2, \ldots$, with some overlapping.

There is actually a transition period, when only the $\mathbf{g}^{(p)}$ with low p are excited, and the support remains close to the origin.

The total enstrophy grows significantly, up to a critical time $T_1 \approx 700\tau$, after which it decreases.

The slides that follow show the main features of the real solution resulting from the computer simulations.

We give the plot of the marginal enstrophy distribution $S_3(k_3, t)$ at $t = 0$ and at $t = T_1 = 711\tau$, $\tau = 1.5625 \times 10^{-8}$, showing that the support moves to the high $|\mathbf{k}|$-region and concentrates around the points $p\mathbf{k}^{(0)} = = (0, 0, pa)$, $p = 0, \pm 1, \pm 2, \ldots$, with some overlapping.

There is actually a transition period, when only the $\mathbf{g}^{(p)}$ with low p are excited, and the support remains close to the origin.

The total enstrophy grows significantly, up to a critical time $T_1 \approx 700\tau$, after which it decreases.
The energy decreases all the time according to the energy identity.

4. Real antisymmetric solutions. Simulations 3

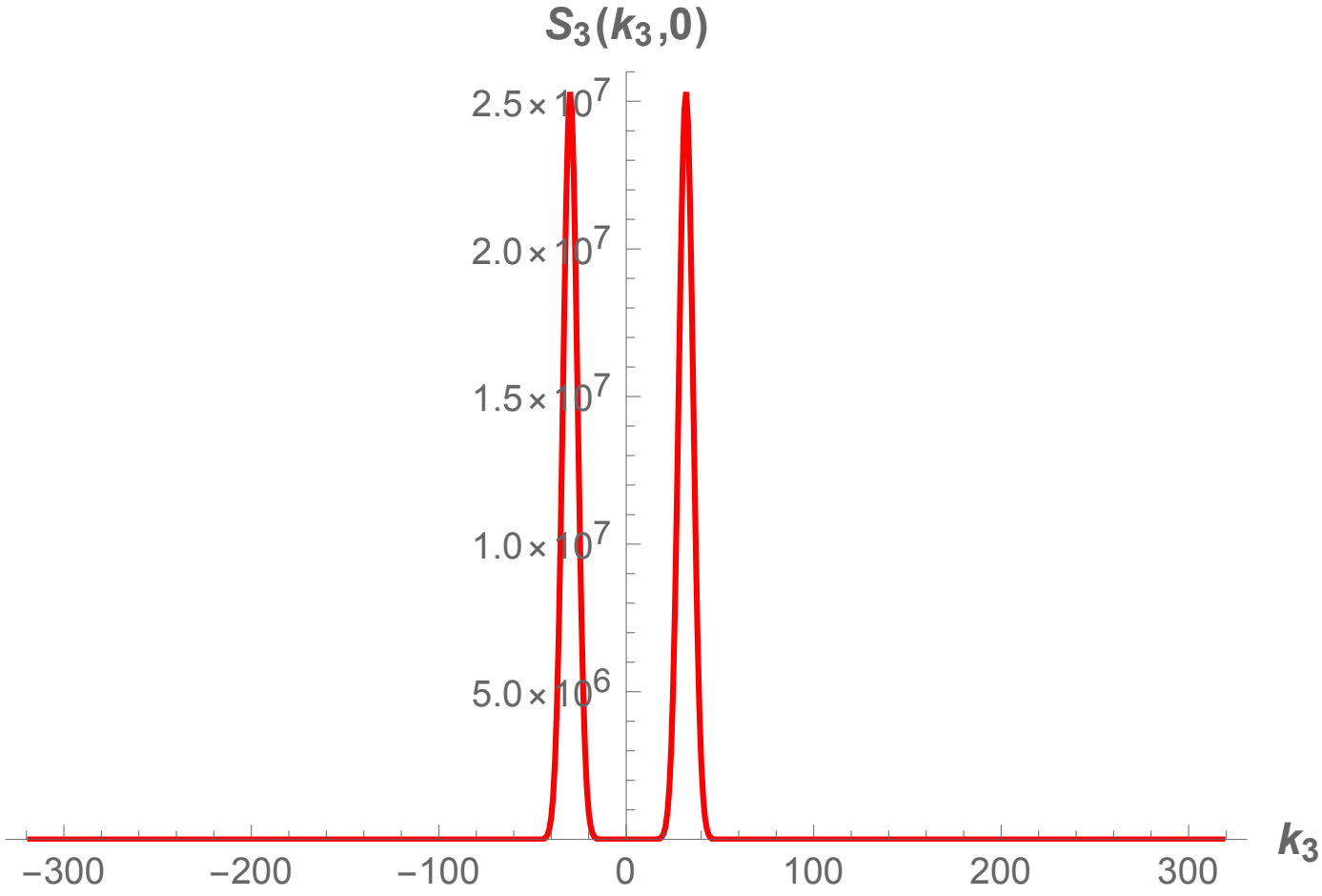

Figure 3: *Plot of the marginal distribution in* $\mathbf{k}$*-space* $S_3(k_3)$ *as at* $t = 0$.

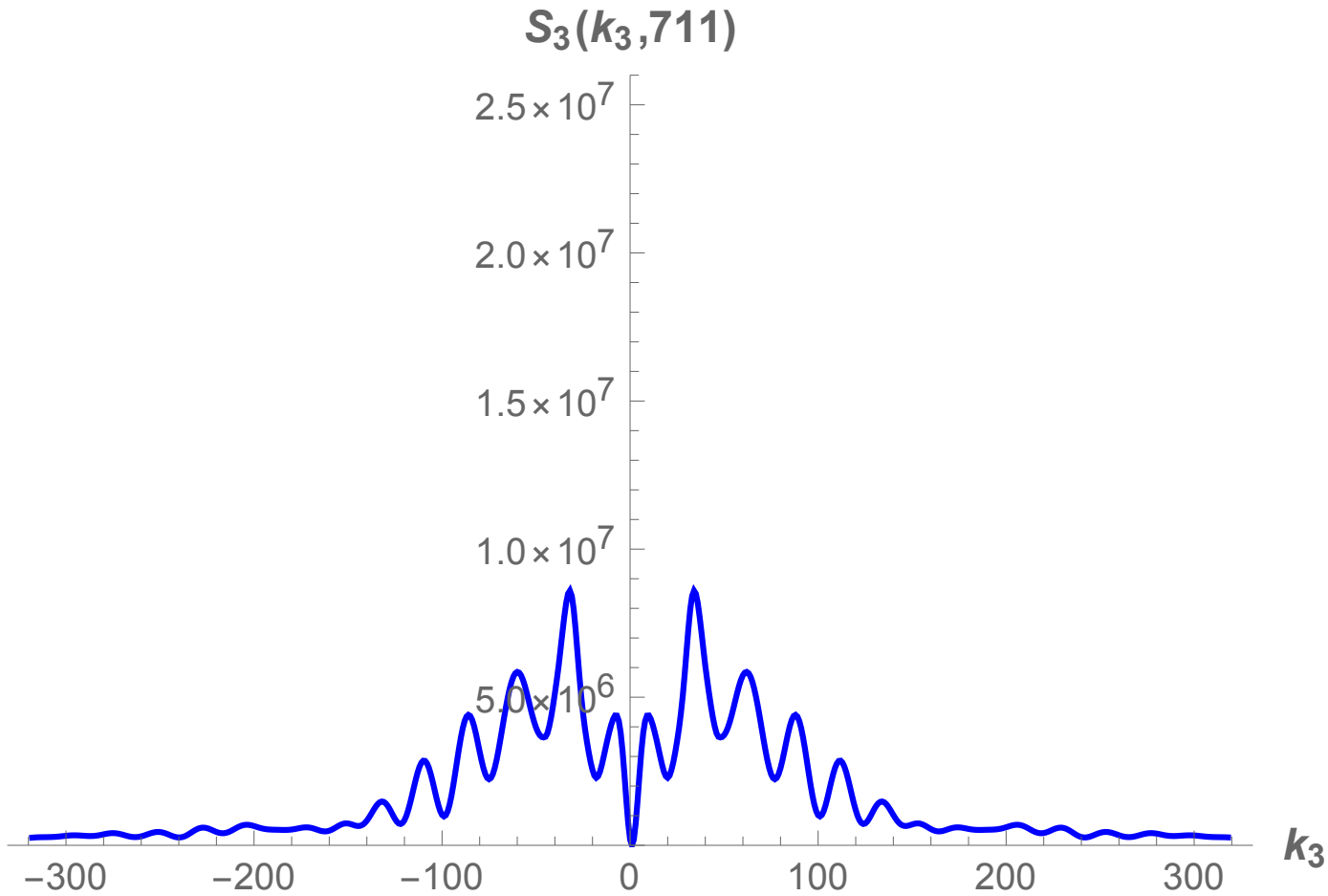

Figure 4: *Plot of the marginal distribution in* $\mathbf{k}$*-space* $S_3(k_3)$ *as at* $t = 711\tau$.

4. Real antisymmetric solutions. Simulations 5

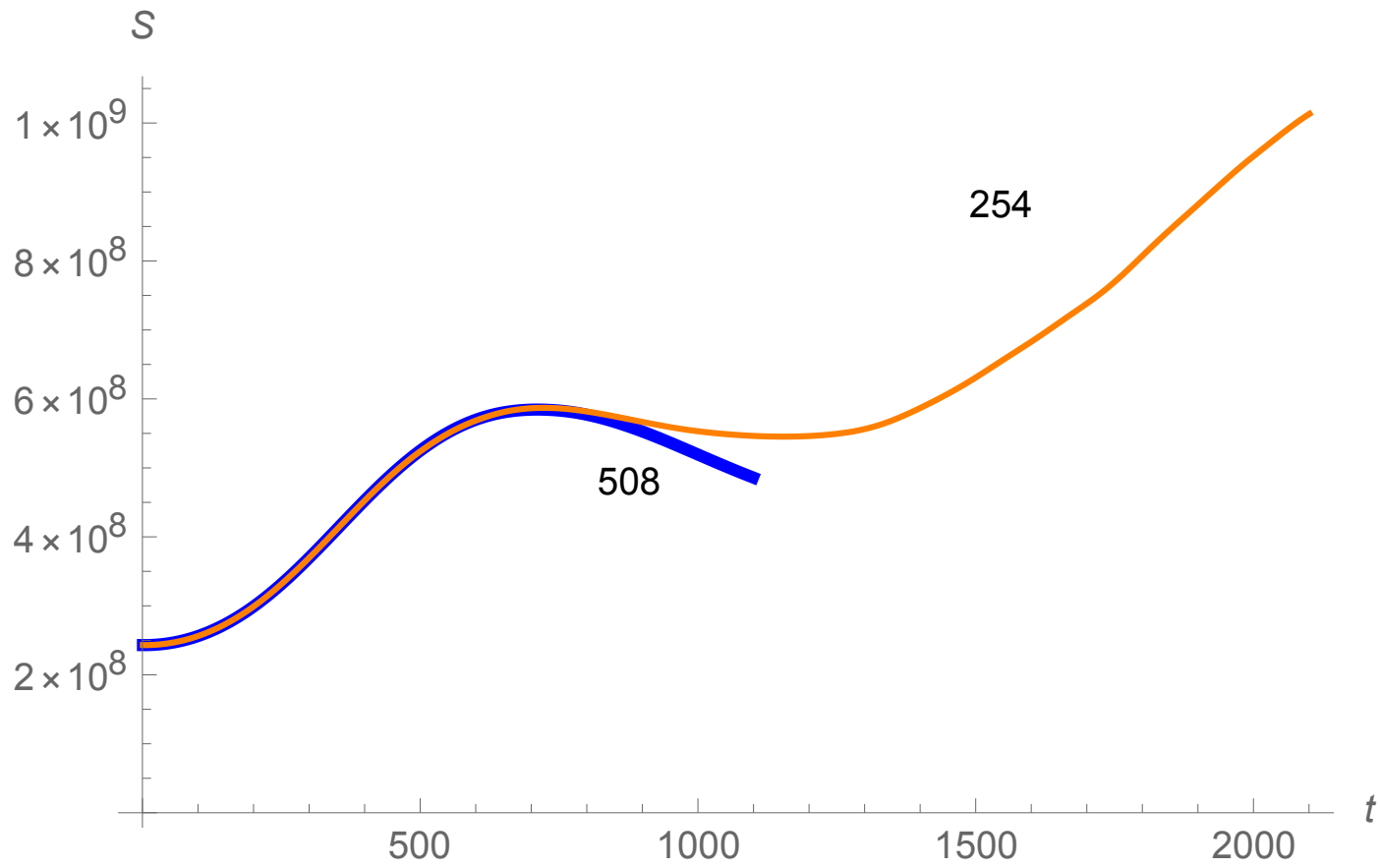

Figure 5: *Plot of the total enstrophy* $S(t)$ *with mesh* $[-147, 147]^2 \times [-3000, 3000]$ *(orange) and with mesh* $[-254, 254]^2 \times [-3000, 3000]$ *(blue). (Time* t *in units* $\tau = 1.5625 \times 10^{-8}$*).*

The previous slide shows a fake blow-up which appears with the narrow mesh $[-147, 157]^2 \times [-3000, 3000]$, due to spurious production of enstrophy at the boundary $k_i = \pm 147$, $i = 1, 2$.

The previous slide shows a fake blow-up which appears with the narrow mesh $[-147, 157]^2 \times [-3000, 3000]$, due to spurious production of enstrophy at the boundary $k_i = \pm 147$, $i = 1, 2$.

Other important features are:

The previous slide shows a fake blow-up which appears with the narrow mesh $[-147, 157]^2 \times [-3000, 3000]$, due to spurious production of enstrophy at the boundary $k_i = \pm 147$, $i = 1, 2$.

Other important features are:

- The maximal velocity $\max_{\mathbf{x}} |\mathbf{u}(\mathbf{x}, t)|$ grows up to a critical time $T_2 \approx 400\tau$, after which it also decreases.

The previous slide shows a fake blow-up which appears with the narrow mesh $[-147, 157]^2 \times [-3000, 3000]$, due to spurious production of enstrophy at the boundary $k_i = \pm 147$, $i = 1, 2$.

Other important features are:

- The maximal velocity $\max_{\mathbf{x}} |\mathbf{u}(\mathbf{x}, t)|$ grows up to a critical time $T_2 \approx 400\tau$, after which it also decreases.

- As time grows $0 < t < T_1$ the largest values of velocity and vorticity concentrate in a kind of torus around the plane $x_3 = \pm \bar{x}_3(t)$,

The previous slide shows a fake blow-up which appears with the narrow mesh $[-147, 157]^2 \times [-3000, 3000]$, due to spurious production of enstrophy at the boundary $k_i = \pm 147$, $i = 1, 2$.

Other important features are:

- The maximal velocity $\max_{\mathbf{x}} |\mathbf{u}(\mathbf{x}, t)|$ grows up to a critical time $T_2 \approx 400\tau$, after which it also decreases.

- As time grows $0 < t < T_1$ the largest values of velocity and vorticity concentrate in a kind of torus around the plane $x_3 = \pm \bar{x}_3(t)$, where $\bar{x}_3(T_2) \approx 0.8$ and $\bar{x}_3(T_1) \approx \frac{\pi}{a}$, corresponding to the natural period $2a$.

The previous slide shows a fake blow-up which appears with the narrow mesh $[-147, 157]^2 \times [-3000, 3000]$, due to spurious production of enstrophy at the boundary $k_i = \pm 147$, $i = 1, 2$.

Other important features are:

- The maximal velocity $\max_{\mathbf{x}} |\mathbf{u}(\mathbf{x}, t)|$ grows up to a critical time $T_2 \approx 400\tau$, after which it also decreases.

- As time grows $0 < t < T_1$ the largest values of velocity and vorticity concentrate in a kind of torus around the plane $x_3 = \pm \bar{x}_3(t)$, where $\bar{x}_3(T_2) \approx 0.8$ and $\bar{x}_3(T_1) \approx \frac{\pi}{a}$, corresponding to the natural period $2a$.

The growth of the maximal velocity and the impressive growth and concentration of vorticity is illustrated by the following slides.

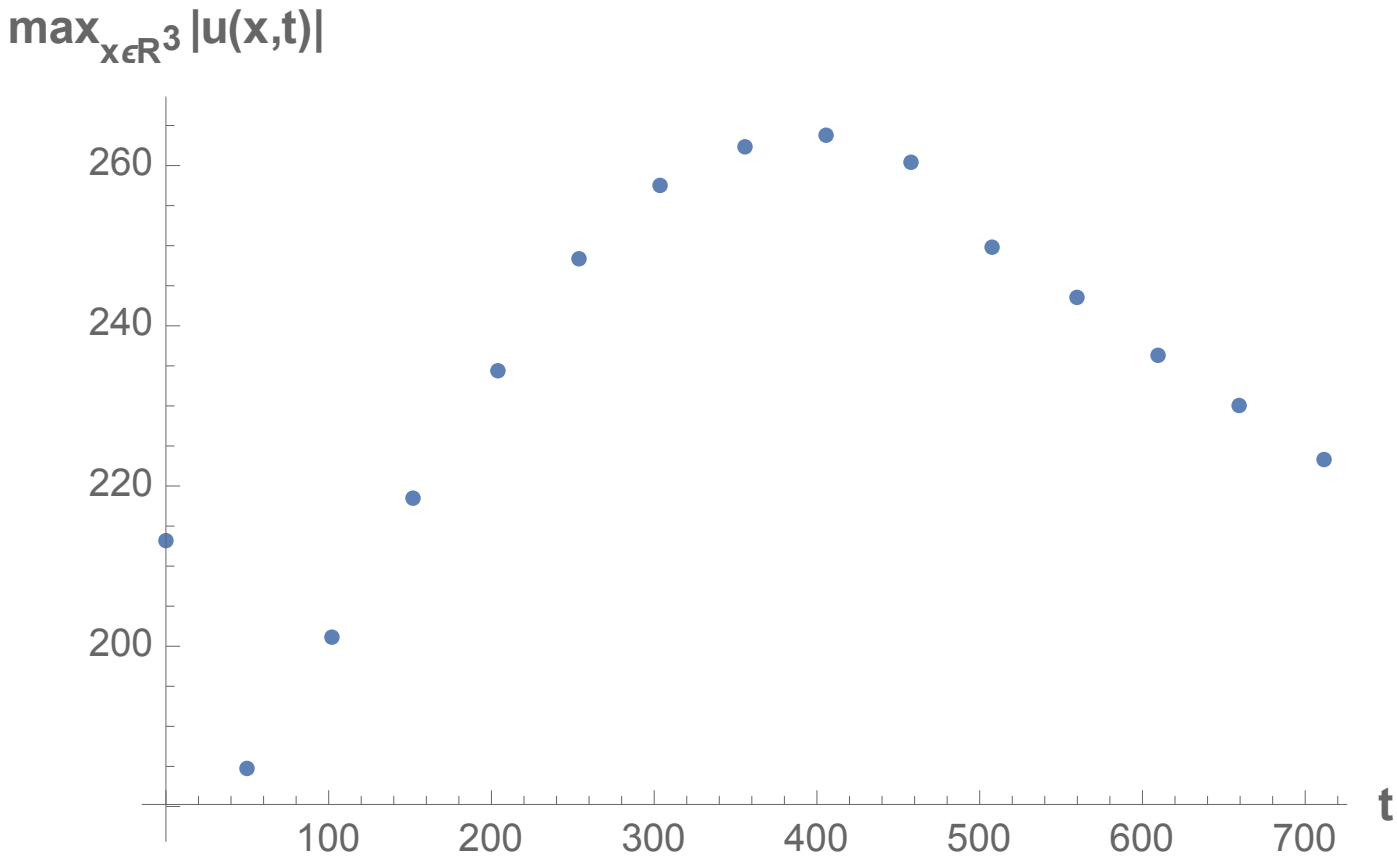

Figure 6: *Plot of the maximal velocity as a function of time (Time t in units $\tau = 1.5625 \times 10^{-8}$).*

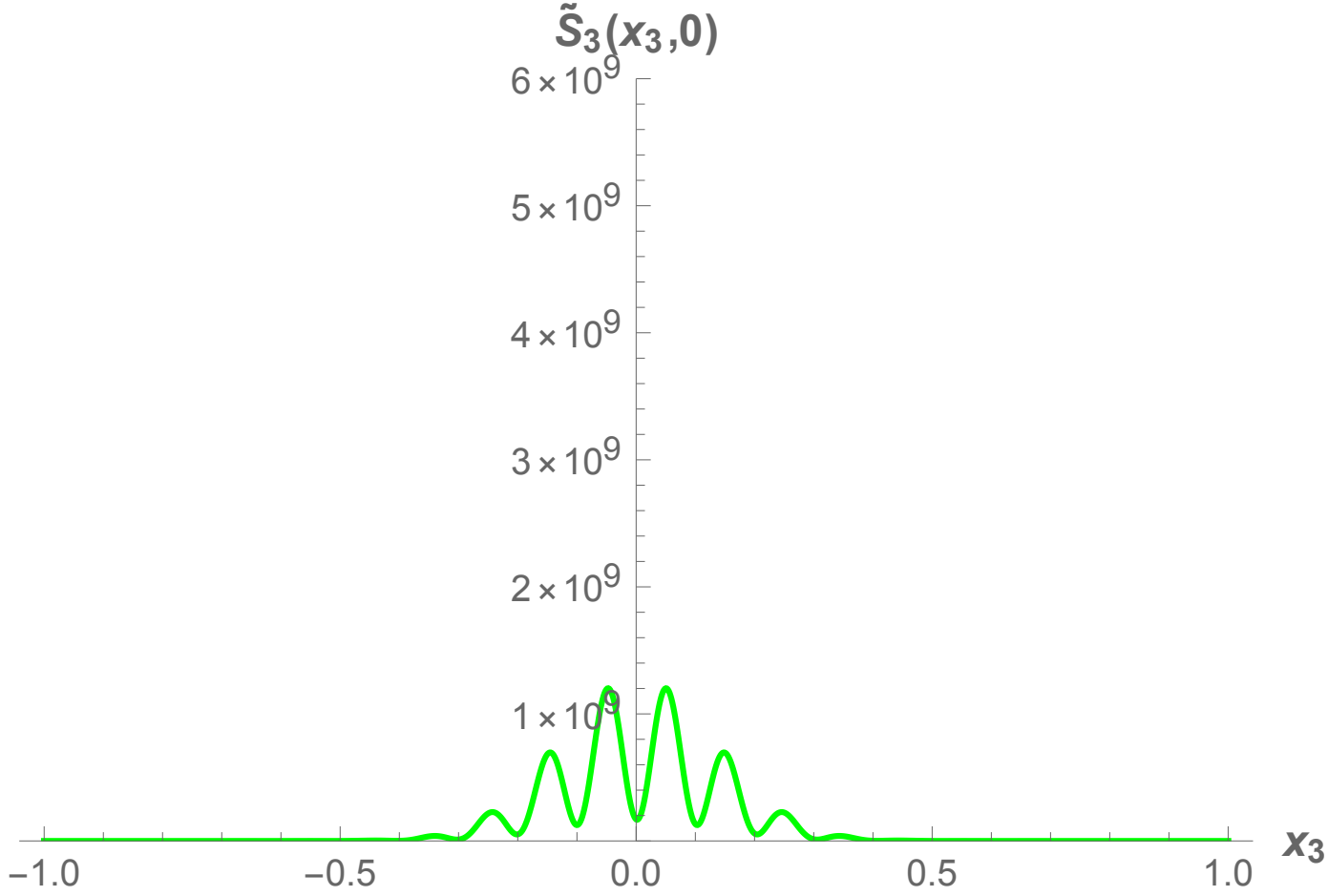

Figure 7: *The marginal distribution* $\tilde{S}_3(x_3, 0)$ *of enstrophy (square modulus of the vorticity) at time* $t = 0$.

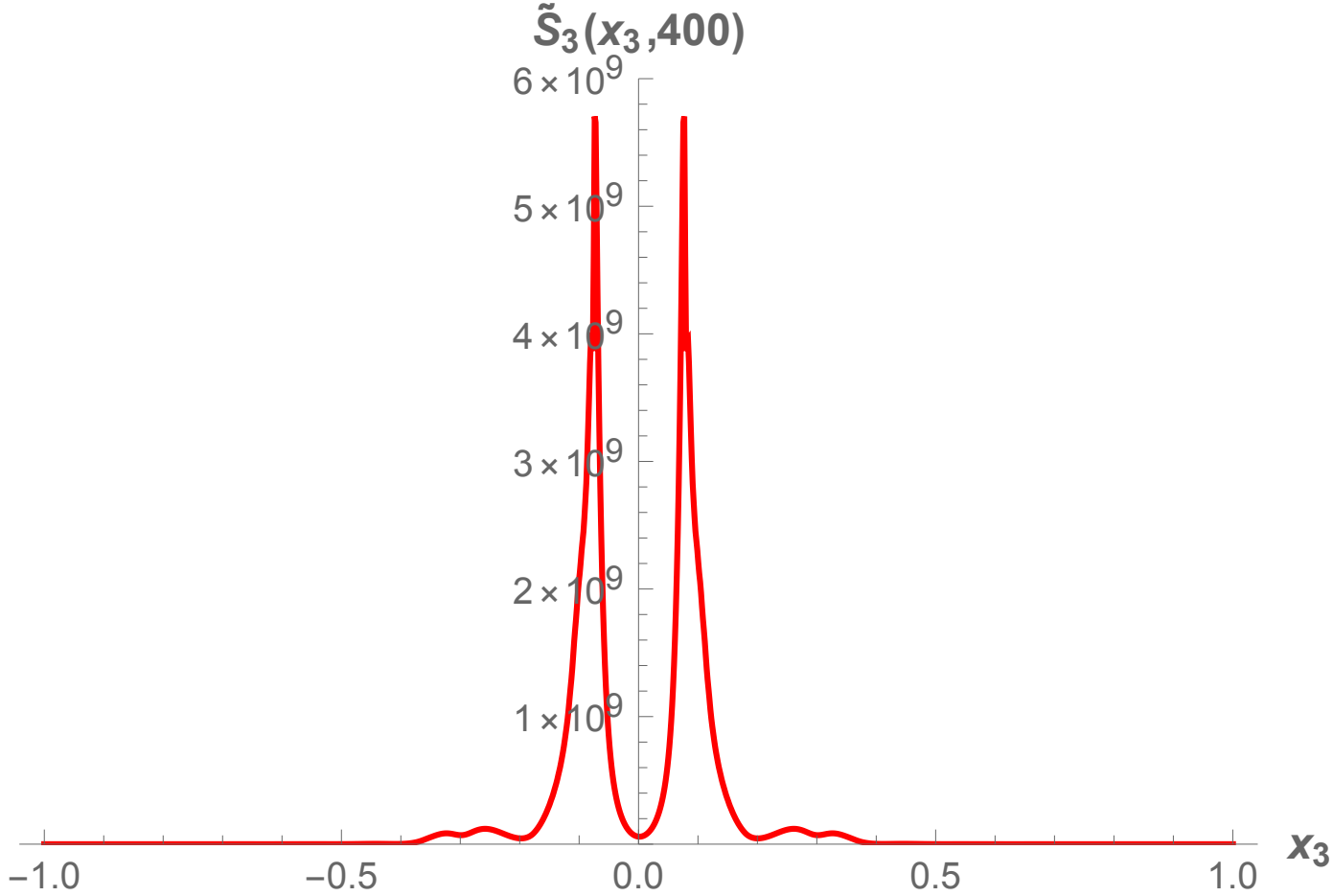

Figure 8: *The marginal distribution* $\tilde{S}_3(x_3, T_2)$ *of enstrophy (square modulus of the vorticity) at time* $t = T_2 \approx 400\tau$. *Vorticity is concentrated in two huge spikes at* $x_3 = \pm\bar{x}_3$, $\bar{x}_3 \approx 0.08$.

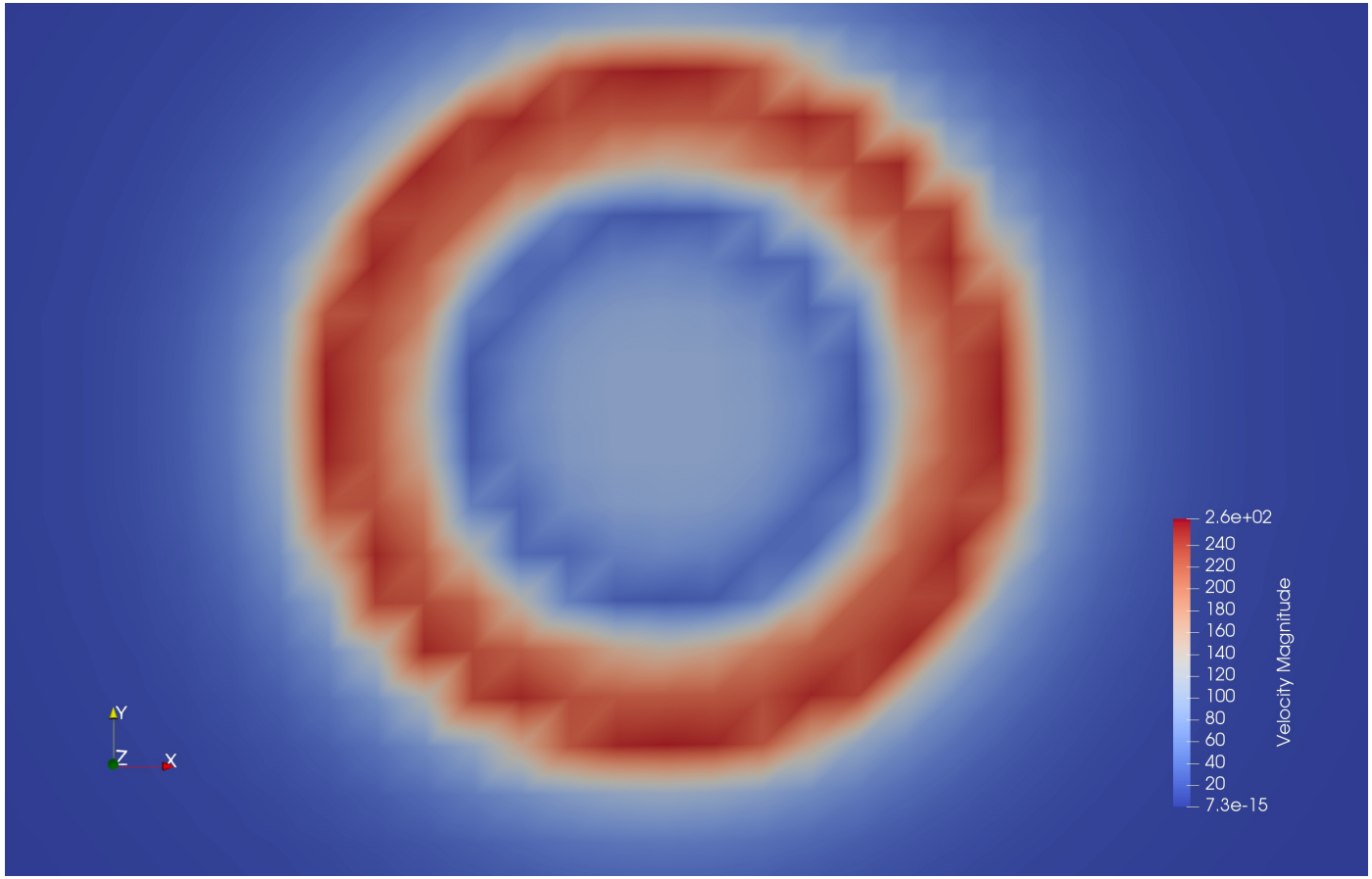

Figure 9: *The velocity magnitude* $|\mathbf{u}(\mathbf{x}, t)|$ *on the plane* $x_3 = 0.08$ *at time* $t = 400\tau \approx T_2$.

5. CONCLUSIONS

The most interesting features of the solutions, as they appear from the simulations are:

5. CONCLUSIONS

The most interesting features of the solutions, as they appear from the simulations are:

- The fast growth of the maximal velocity and of the total vorticity;

5. CONCLUSIONS

The most interesting features of the solutions, as they appear from the simulations are:

- The fast growth of the maximal velocity and of the total vorticity;

- The concentration up to time T_1 of the large velocities and vorticities in two symmetric annular regions with symmetry planes $x_3 = \pm\bar{x}_3(t)$, while elsewhere the fluid remain quiet.

5. CONCLUSIONS

The most interesting features of the solutions, as they appear from the simulations are:

- The fast growth of the maximal velocity and of the total vorticity;

- The concentration up to time T_1 of the large velocities and vorticities in two symmetric annular regions with symmetry planes $x_3 = \pm\bar{x}_3(t)$, while elsewhere the fluid remain quiet.

Both features recall the behavior of tornadoes or hurricanes.

Concerning the GRP, it is unlikely that solutions described above, related to the fixed point $\mathbf{H}^{(0)}$ can become singular.

Concerning the GRP, it is unlikely that solutions described above, related to the fixed point $\mathbf{H}^{(0)}$ can become singular.

In fact, $\mathbf{H}^{(0)}$ is axial symmetric with zero swirl, and the initial data are also close to that.

Concerning the GRP, it is unlikely that solutions described above, related to the fixed point $\mathbf{H}^{(0)}$ can become singular.

In fact, $\mathbf{H}^{(0)}$ is axial symmetric with zero swirl, and the initial data are also close to that.

It is well known that if a NS solution is axial symmetric with zero swirl, or close to that, global regularity holds (*Z. Lei & Q. Zang 2017*).

Concerning the GRP, it is unlikely that solutions described above, related to the fixed point $\mathbf{H}^{(0)}$ can become singular.

In fact, $\mathbf{H}^{(0)}$ is axial symmetric with zero swirl, and the initial data are also close to that.

It is well known that if a NS solution is axial symmetric with zero swirl, or close to that, global regularity holds (*Z. Lei & Q. Zang 2017*).

Further work is needed in order to understand the behavior of the flows with initial data leading to fixed points which are not axial symmetric or axial symmetric with swirl.

REFERENCES

1) C. B., D. Li & Ya.G. Sinai:"Complex singular solutions of the 3-d Navier-Stokes equations and related real solutions". Journal of Statistical Physics, vol. 167, n. 1, pagg. 1-13, DOI 10.1007/s10955-017-1730-1 (2017)

2) C.B., S. Frigio & P. Maponi, P. :"On the blow-up of some complex solutions of the 3D Navier-Stokes Equations: theoretical predictions and computer simulations." IMA Journal of Mathematical Physics vol. 83 pag 697-714; doi: 10.1063/1.4746814 (2017)

3) A. Cheskidov: "Blow-up in finite time for the dyadic model of the Navier-Stokes equations". Trans. Am. Math. Soc., 10, 5101-5120.

4) Z. Lei & Q. Zang: "Criticality of the axially symmetric Navier-Stokes equations". Pacific Journal of Mathematics, 289, 169-187 (2017)

5) D. Li & Ya. G. Sinai: "Blowups of complex solutions of the 3D Navier-Stokes system and renormalization group method". J. Eur. Math. Soc., 10, 267-313. (2008)
6) D. Li & Ya. G. Sinai: "Blowups of Complex-valued Solutions for Some Hydrodynamic models". Regular and Chaotic Dynamics, 15, Nos 4-5, 521-531 (2010).
7) N. H. Katz & N. Pavlovic "Finite time blow-up for a dyadic model of the Euler equations". Transactions of AMS 357, No. 2 (2005), 695–708,
8) G. Seregin: "A Certain Necessary Condition of Potential Blow up for Navier-Stokes Equations". Commun. Math. Phys. vol. 312, 833-845, (2012) .
9) T. Tao "Finite time blowup for an averaged three-dimensional Navier-Stokes equation". J. Amer. Math. Soc. 29 (2016), no. 3, 601-674, (2016)

THANK YOU FOR YOUR ATTENTION